



TALLINNA TEHNIKAÜLIKOOL  
TALLINN UNIVERSITY OF TECHNOLOGY

---

Department of Materials and Environmental Technology

Investigation of potassium doping on  $\text{Cu}_2(\text{Zn,Cd})\text{SnS}_4$   
monograin powder properties

Kaaliumi mõju uurimine  $\text{Cu}_2(\text{Zn,Cd})\text{SnS}_4$  monoterapulbri omadustele

MASTER THESIS

LASISI I. ADEKUNLE

KAYM156322

Supervisor: Dr. Marit Kauk-Kuusik  
Senior Research Scientist

Co-supervisor: Dr. Kristi Timmo  
Senior Research Scientist

Tallinn, 2017

## AUTHOR'S DECLARATION

Hereby I declare, that I have written this thesis independently.  
No academic degree has been applied for based on this material.  
All works, major viewpoints and data of the other authors used in this thesis have been referenced.

“.....” ..... 201.....

Author: .....  
/signature /

Thesis is in accordance with terms and requirements

“.....” ..... 201.....

Supervisor: .....  
/signature/

Accepted for defence

“.....” .....201....

Chairman of theses defence commission: .....  
/name and signature/

# TABLE OF CONTENT

List of Abbreviations and Symbols.....	5
INTRODUCTION.....	6
<b>1. LITERATURE REVIEW.....</b>	<b>8</b>
<b>1.1 PHOTOVOLTAIC CELL.....</b>	<b>8</b>
1.1.1 Structure and working principle.....	8
1.1.2 <i>p-n</i> junction formation.....	9
1.1.3 Efficiency loss in <i>p-n</i> junction.....	9
<b>1.2 Semiconductor compounds as absorber materials for photovoltaics.....</b>	<b>10</b>
1.2.1 Kesterite absorber materials.....	11
1.2.2 Monograin layer solar cells.....	12
1.2.2.1 Growth of $\text{Cu}_2\text{ZnSnS}_4$ monograin powders.....	13
1.2.2.2 Formation of $\text{Cu}_2\text{ZnSnS}_4$ .....	13
1.2.2.3 Thermal treatment.....	15
1.2.3 Defects of quaternary compounds.....	16
1.2.4 Metal ion substitution in $\text{Cu}_2\text{ZnSnS}_4$ .....	17
1.2.5 Doping.....	18
1.2.5.1 Effects of alkali metals doping to the solar cell absorber materials.....	19
<b>1.3 Summary of literature review and objective of study.....</b>	<b>19</b>
<b>2. EXPERIMENTAL PROCEDURE.....</b>	<b>21</b>
<b>2.1 Preparation of <math>\text{Cu}_2(\text{Zn,Cd})\text{SnS}_4</math> monograin layer solar cell.....</b>	<b>21</b>
2.1.1 Growth of monograin powders.....	22
2.1.2 Chemical etching.....	22
2.1.3 $\text{Cu}_2(\text{Zn,Cd})\text{SnS}_4$ doping with potassium.....	22
2.1.3.1 K-doping from the solution.....	22
2.1.3.2 Doping by recrystallization method.....	23
2.1.4 Buffer layer by Chemical Bath Deposition.....	24
2.1.5 Window layer deposition and formation of back contacts.....	25
<b>2.2 Characterization of monograins and solar cells.....</b>	<b>25</b>
2.2.1 Current-voltage characteristics of solar cells.....	26

<b>3. RESULTS AND DISCUSSION.....</b>	<b>27</b>
<b>3.1 Elemental composition.....</b>	<b>27</b>
3.1.1 Composition of $\text{Cu}_2\text{Zn}_{1-x}\text{Cd}_x\text{SnS}_4$ crystals synthesized in $\text{CdI}_2$ flux .....	27
3.1.2 Composition of $\text{Cu}_2\text{Zn}_{1-x}\text{Cd}_x\text{SnS}_4$ crystals recrystallized in KI flux.....	28
3.1.3 Surface composition by XPS.....	29
<b>3.2 Structural study of K-doped <math>\text{Cu}_2\text{Zn}_{1-x}\text{Cd}_x\text{SnS}_4</math> monograin powders .....</b>	<b>31</b>
3.2.1 Raman spectroscopy analysis.....	31
<b>3.3 Morphology of <math>\text{Cu}_2\text{Zn}_{1-x}\text{Cd}_x\text{SnS}_4</math> monograin powder crystals .....</b>	<b>32</b>
<b>3.4 Photoluminescence study .....</b>	<b>33</b>
<b>3.5 Device characterization.....</b>	<b>35</b>
<b>CONCLUSIONS.....</b>	<b>39</b>
<b>ABSTRACT .....</b>	<b>40</b>
<b>RESÜMEE .....</b>	<b>41</b>
<b>REFERENCES .....</b>	<b>43</b>
<b>ACKNOWLEDGEMENT .....</b>	<b>48</b>

## LIST OF ABBREVIATIONS AND SYMBOLS

CZTS -  $\text{Cu}_2\text{ZnSnS}_4$

CZTSe -  $\text{Cu}_2\text{ZnSnSe}_4$

CZTSSe –  $\text{Cu}_2\text{ZnSn}(\text{S},\text{Se})_4$

CZCdTS -  $\text{Cu}_2(\text{Zn},\text{Cd})\text{SnS}_4$

CIS -  $\text{CuInSe}_2$

CIGS -  $\text{Cu}(\text{In},\text{Ga})\text{Se}_2$

CdTe - Cadmium Telluride

CGS -  $\text{CuGaS}_2$

CdS - Cadmium Sulfide

CBD - Chemical Bath Deposition

CBO - Conduction Band Offset

$E_g$  - Band gap

$FF$  - Fill factor

$I$ - $V$  - Current-voltage

$J_{sc}$  - Short-circuit current density

$V_{oc}$  - Open circuit voltage

KCN -Potassium cyanide

MGL - Monograin layer solar cell

$\eta$  - Solar cell efficiency

PV - Photovoltaic

SEM - Scanning electron microscopy

TFSC - Thin film solar cell

TW - Terawatt

TU - Thiourea

## INTRODUCTION

An expected increase in world population will inevitably lead to an increase in energy demand as undeveloped and developing parts of the world continue to deploy machinery for infrastructural development. The current annual global energy demand of 10 terawatt (TW) is expected to be one third of the demand by 2050 [1]. To avoid increasing the level of CO<sub>2</sub> emission into the atmosphere from traditional sources of energy by meeting this overwhelming energy demand, alternative sources of energy must be considered [1, 2]. Amongst the renewable energy sources, solar has the highest potential to play a significant role in world energy security due to its largely underutilized abundant resource [3].

Solar cells are semiconductor based compounds that absorb photons from solar radiation to produce electron-hole pairs which are then separated by the *p-n* junction [4, 5]. The production of solar cells has evolved over the years from the choice of materials to the technology deployed in making the cells [5–8]. The first generation of solar cells are made from silicon and these include monocrystalline silicon cell, polycrystalline silicon cell, and hybrid silicon cells [3, 5, 7]. The second generation of solar cells are generally known as thin film solar cells (CIGS, CdTe etc.) while the third generation includes variety of new materials besides silicon, including nanotubes, silicon wires, solar inks using conventional printing press technologies, organic dyes, and conductive plastics [5, 7].

The excessive cost of solar cells has been the main obstacle of solar energy in competing with other sources of energy. To overcome this obstacle, there has been a lot of interest in monograin technology which involves the use of powders to form absorber layers of solar cells and has the advantage of making large areas that are single crystalline layers [9]. Monograin technology is considered due to its low cost, simplicity of the materials and device technology, and the possibility of making flexible devices as well as using up 100% of the material.

The last decade has witnessed remarkable progress in photovoltaic applications using kesterite absorbers, with steady improvement in power conversion efficiency (PCE) from ~5% in 2004 to 12.7% in 2014 [10, 11]. Amongst kesterites, Cu<sub>2</sub>ZnSn(S,Se)<sub>4</sub> (CZTSSe) has received a lot of attention recently due to its constituents being abundant, cheap and nontoxic [12, 13]. The presence of more defects and impurities in CZTSSe than those of binary and ternary

semiconductors is responsible for its lower efficiency when compared to the others, and this is traceable to its structure of five component elements [14]. To mitigate this effect several researchers have investigated various aspects of kesterite based semiconductors. One of the areas of research focus has been doping, while there are several reports on the influence of doping with alkali metals in thin film solar cells, there are very few reports on doping monograin powders [15, 17].

The aim of this study was to investigate the influence of potassium doping on  $\text{Cu}_2(\text{Zn,Cd})\text{SnS}_4$  monograin powder properties and on monograin layer solar cell parameters. For doping, two methods were used: solution based doping method and  $\text{Cu}_2(\text{Zn,Cd})\text{SnS}_4$  recrystallization in potassium iodide (KI). The thesis is based on the experimental work carried out in the Laboratory of Photovoltaic Materials at the Department of Materials and Environmental Technology, Tallinn University of Technology.

# 1. LITERATURE REVIEW

## 1.1 PHOTOVOLTAIC CELL

### 1.1.1 Structure and working principle

Photovoltaic (PV) cells also known as solar cells are electronic devices that convert solar energy into electrical energy by photovoltaic effect, which is the creation of voltage or electric current by semiconductors in contact upon exposure to light. Figure 1.1 shows the working principle of the photovoltaic cell.

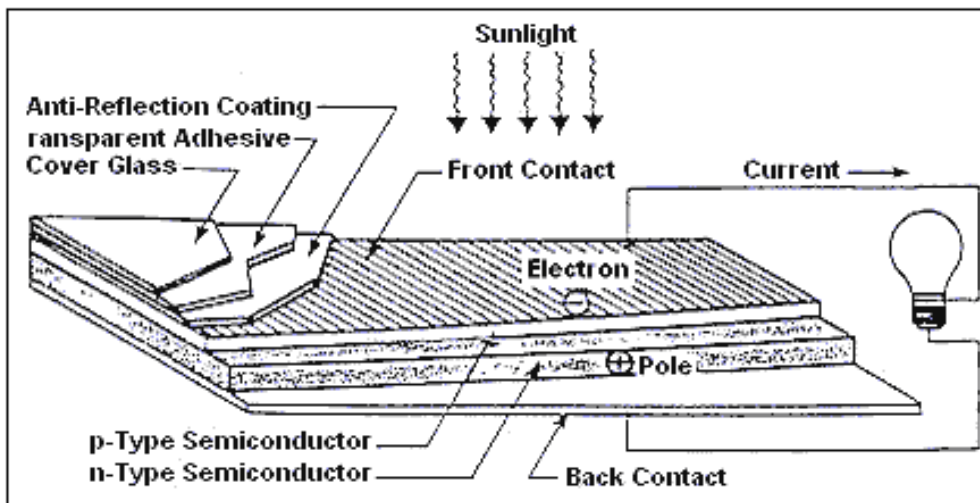


Figure 1.1 Photovoltaic cell [18].

Electron-hole pairs are generated by the photon of light in the contact area of the *p*- and *n*-type semiconductors called *p-n* junction. The movement of the electrons to the negative terminal and holes to the positive terminal generates the electrical power, which is dissipated into the circuit [19]. While a variety of materials satisfy the basic requirement for photovoltaic energy conversion, semiconductor materials are widely used to form *p-n* junction in photovoltaic energy conversion devices [20]. For solar cell operations, a semiconductor must have a bandgap of 1.0–1.7 eV and must be able to generate and recombine electrons and holes upon impact by photon. It takes photons with energy higher than or equal to the band gap energy to excite the valence electrons [21].

### 1.1.2 *p-n* junction formation

A solar cell among others consists of 2 types of semiconductors, *n-type* semiconductor (carrier of excess electrons) and *p-type* semiconductor (carrier of excess holes) that come in contact to form the *p-n* junction (shown in Figure 1.2). During the operation of a solar cell, the electrons excited from the conduction band flow from the *p-type* to the *n-type* side, while there is flow in the opposite direction by the holes left in the valence band [22]. This is the diffusion that occurs over time to cause equal distribution of charges within the system [23]. As they cross the junction, the fixed ions they leave behind establish an electric field that separates them at the *p-n* junction [19, 20].

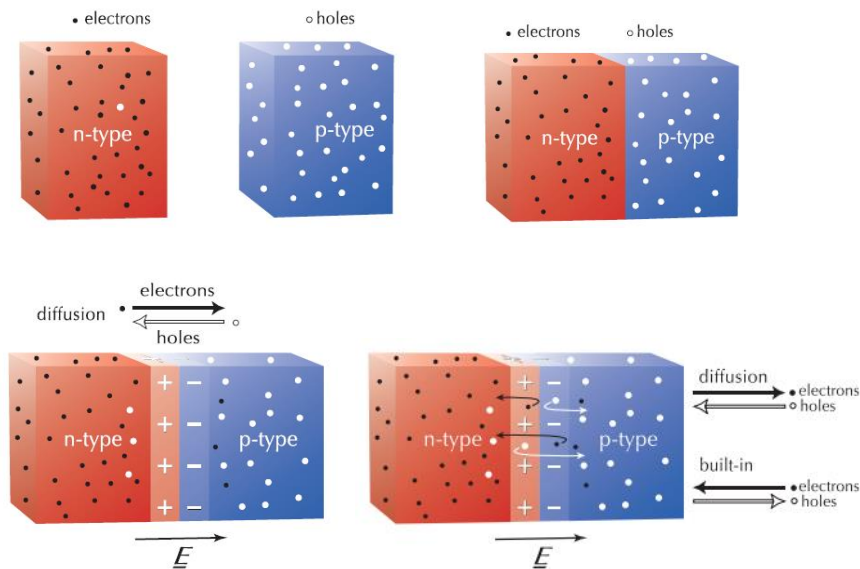


Figure 1.2 Stages in formation of a *p-n* junction [23].

### 1.1.3 Efficiency loss in *p-n* junction

There are four efficiency loss processes identified in the *p-n* junction: 1) thermalization loss; 2) junction loss; 3) contact loss; and 4) recombination loss as depicted in Figure 1.3 below [22].

- *Thermalization loss*: This is the rapid loss of excess energy by the photoexcited electron-hole pairs above the band gap.

- *Contact losses*: The transmission of electric current produced by the solar cell involves ohmic losses. These can also be considered as a resistance in the equivalent circuit. It is seen that the series resistance affects the cell operation mainly by reducing the fill factor.

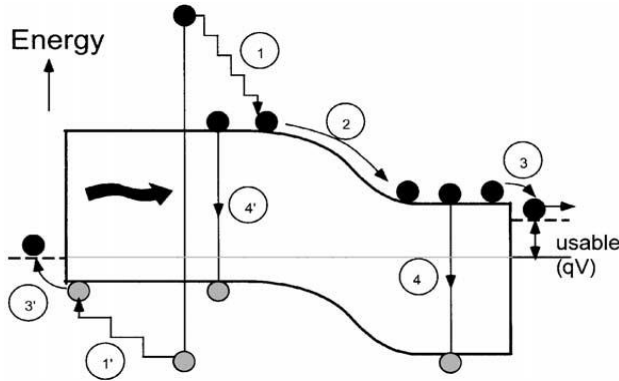


Figure 1.3 Losses in *p-n* junction [22].

- *Recombination loss*: Recombination is most common when an electron-hole pair is converted into radiant energy. Recombination is most common at impurities or defects of the crystal structure, or at the surface of the semiconductor where energy level may be introduced inside the energy gap. These levels act as stepping stones for the electrons to fall back into the valence band and recombine with holes. Surface recombination and recombination at contacts reduces both solar cell output parameters: the open circuit voltage and short circuit current.

## 1.2 Semiconductor compounds as absorber materials for photovoltaics

Absorber materials for solar cell applications should be made from semiconductors that have a direct bandgap within the acceptable range of 1.0-1.7 eV and high absorption coefficient of  $10^4 \text{ cm}^{-1}$  in the visible region [6, 21, 22]. The absorber materials used for solar cells are classified into three main groups: silicon, inorganic compounds and organic semiconductor materials. The inorganic semiconductor materials used for photovoltaic cells include silicon (mono-crystalline, polycrystalline, amorphous and microcrystalline), the III-V group compounds and alloys, CdTe and the chalcopyrite compounds, copper indium gallium diselenide (CIGS) [25]. There has been a decline in the use of monocrystalline silicon as seen in Figure 1.4 below.

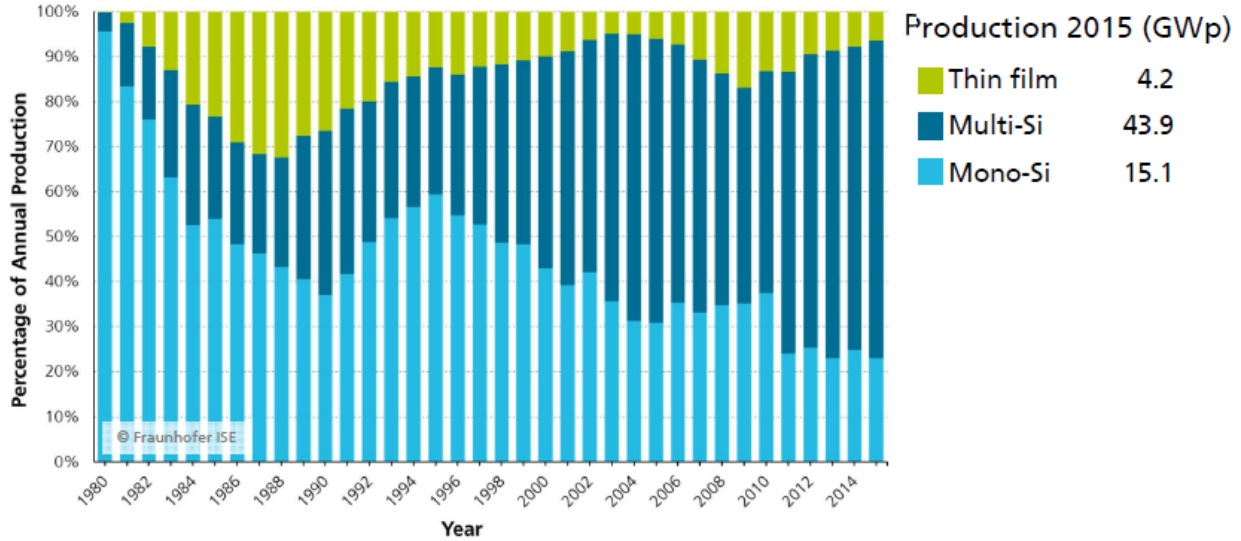


Figure 1.4 PV production by technology [26].

### 1.2.1 Kesterite absorber materials

The presence of constituents that are naturally abundant, inexpensive and non-toxic makes kesterites very attractive for solar cell applications [6, 14, 24–27]. Quaternary compounds such as  $\text{Cu}_2\text{ZnSnS}_4$  (CZTS) and  $\text{Cu}_2\text{ZnSnSe}_4$  (CZTSe), have optical and electronic properties comparable to  $\text{Cu}(\text{In,Ga})(\text{S,Se})_2$  (CIGS) and  $\text{CdTe}$  [29]. To reduce the production cost as a result of expensive materials and eliminate environmental impact of toxic materials, CZTS is an ideal candidate to replace  $\text{Cu}(\text{In,Ga})\text{Se}_2$  (CIGS) and  $\text{CdTe}$  for large scale production of solar cells [31].  $\text{Cu}_2\text{ZnSnS}_4$  is one of the I-II-IV-VI group materials that can be derived from  $\text{CuInS}_2$  by substituting In (III) with Zn (II) and Sn (IV) [32]. CZTS has a high absorption coefficient of  $>10^4 \text{ cm}^{-1}$  and band gap energy of 1.4 eV to 1.5 eV, making it suitable for photovoltaics application [6, 22, 26]. Timmo *et al.* reported that the bandgap of CZTS can be altered to get better solar cell characteristics by partially substituting S with Se [33]. The preparation of CZTS absorber thin films can be by vacuum and non-vacuum based methods. The vacuum based methods are used for controlling deposition parameters to obtain desired stoichiometric ratio and crystalline quality, while non-vacuum methods are mainly adopted for reducing material cost and are simplified methods for production [32].

Also, indium free quaternary semiconductor CZTS thin film, is an ideal alternative to CIGS solar cells, due to its nearly optimal direct band gap energy of 1.5 eV and inherent high absorption coefficient ( $10^4 \text{ cm}^{-1}$ ) [34]. Its fabrication processes, physical properties similar to those of CIGS

as well as the low cost and abundance of the constituent elements zinc (Zn) and tin (Sn) make it attractive for photovoltaic applications [34].

### 1.2.2 Monograin layer solar cells

The production of solar cells in the photovoltaic industry has been done primarily by using wafers of single-crystal and polycrystalline silicon, which generally have thickness within the range of 100–300  $\mu\text{m}$  [35]. The wafers go through several processing steps before integration into modules, which are relatively expensive due to the high material and processing costs [35]. For solar cells to remain competitive in the market, cheaper materials and synthesis processes must be considered. The most attractive of the solar cells is the monograin layer (MGL) solar cell, which combines features of monocrystalline solar cell and thin film solar cell. Monograin powder technology is considered due to its low cost, simplicity of the materials and device technology, and the possibility of making flexible devices as well as using up 100% of the material [9, 10]. It permits the fabrication of large-area modules at room temperature in a continuous roll-to-roll process, and the homogeneous composition of powders gives an additional advantage, leading to homogeneous modules without any up-scaling problem [10].

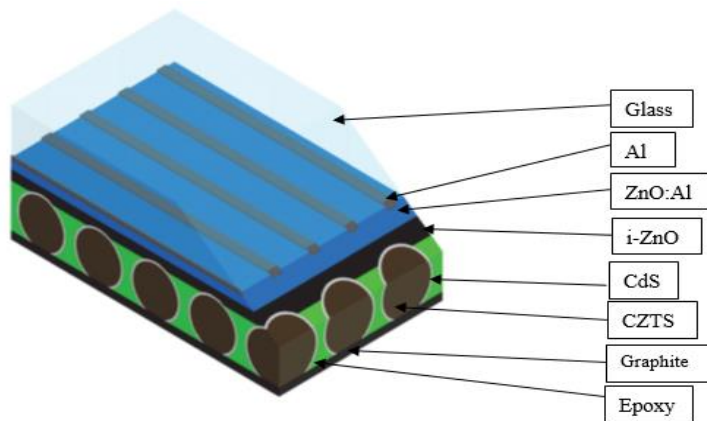


Figure 1.5 Schematic structure of monograin layer solar cell [37].

The photoactive layer is formed from a *p-type* semiconductor material such as  $\text{Cu}_2\text{ZnSnS}_4$  (CZTS) or  $\text{CuInSe}_2$  (CIS), with single crystalline grains embedded into an organic resin (epoxy) [36]. Uniform fractions of the grown powder crystals are covered with CdS buffer layer by chemical bath deposition. This is followed by RF-sputtering of i-ZnO and conductive ZnO:Al

layers on the open surface before the highly conductive grid contacts are deposited on top of the ZnO layer, and the structure is glued onto a glass substrate for durability. The back-contact areas of the crystals that are originally inside the epoxy are opened by etching the epoxy with  $H_2SO_4$  for the appropriate time and then polished with sandpaper. Back contacts are made using graphite paste and the monograin layer solar cell is ready for analysis. Figure 1.5 shows the schematic structure of monograin layer solar cell.

This method is beneficial because it allows the control of the chemical composition and the size of the powder grains as well as makes use powders with single-crystalline structure that promotes uniform distribution of doping impurities and have narrow granulometric composition [38]. The monograin layer (MGL) technology allows the separation of fabrication of absorber/junction formation and cell/module formation.

#### **1.2.2.1 Growth of $Cu_2ZnSnS_4$ monograin powders**

Generally, monograin powders can be synthesized from either their abundant pure elements, their binaries or from intermetallic compounds in the presence of liquid phase of used flux material. Single-crystalline powders of CZTS can be obtained at temperatures above the melting point of the used salt (flux). The use of molten salts as flux in synthesis process is to enhance the rate of solid-state reactions due to the much higher diffusion rates between reaction components in the molten media, lowering the reaction temperature, increasing the homogeneity of the solid product, and controlling the particle size and shape as well as their agglomeration state [10]. A good flux material should have low melting temperature, low vapor pressure and high solubility in water, allowing for easy separation of the crystals from it [10]. The use of water soluble salts such as KI, NaI and  $CdI_2$  for the synthesis of monograin powder has been reported in literature [15, 16, 39, 40]. The quantity of the used flux material should exceed the amount of flux sufficient to fill all the empty space between initial precursor particles to avoid particle sintering by repelling the precursor particles and the formed single crystalline monograins from each other[4].

#### **1.2.2.2 Formation of $Cu_2ZnSnS_4$**

The formation of  $Cu_2ZnSnS_4$  from binary precursors has been reported to start with a decrease in the CuS and SnS phase based on Raman and XRD investigations [41].  $Cu_2S$ ,  $SnS_2$  and S peaks

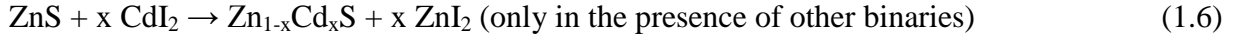
were observed in XRD at 270 °C, while the sample consisted of metallic phases of Cu<sub>6</sub>Sn<sub>5</sub> and Cu<sub>3</sub>Sn in addition to the binary sulfides at 350 °C. CZTS peaks were observed at 470 °C alongside ZnS, CuS and Cu<sub>2-x</sub>S. The CZTS peak became the dominant peak at 530 °C, but a weak peak of Cu<sub>2</sub>S remained in spectra. The CZTS peak was sharp and distinct at 580 °C. Raman analysis reveals that intermediate ternary phases such as Cu<sub>2</sub>SnS<sub>3</sub>, Cu<sub>4</sub>SnS<sub>4</sub> and Cu<sub>4</sub>SnS<sub>6</sub> exist prior to the formation of Cu<sub>2</sub>ZnSnS<sub>4</sub>. The main reaction paths for Cu<sub>2</sub>ZnSnS<sub>4</sub> formation are presented in equations 1.1-1.3 [41].



Muska *et al.* reported that the elemental composition of the precursors used for synthesis affect the final composition of the CZTS monograin powder grown in KI [42]. The authors' investigation revealed that in slightly Zn-rich conditions (Zn/Sn=1.03), the increase in the ratio of [Cu]/([Zn]+[Sn]) in the precursor mixture decreased the ratio of [Zn]/[Sn] from 1.03 to 0.92 in the final product, while an increase in the ratio of [Cu]/([Zn]+[Sn]) in precursors to over 0.95, yielded Sn-rich and Cu-rich powder. It was found that, in these growth conditions, secondary phases such as Cu- and Sn-binaries and Cu<sub>2</sub>SnS<sub>3</sub> were formed together with quaternary compound. However, in Zn-rich growth conditions (1.03<Zn/Sn≤1.2) with constant Cu content in precursors, the composition of formed CZTS powder crystals was not affected. This increased the ZnS secondary phase by the addition of Zn in the precursors' mixture. On the other hand, Zn-poor growth conditions (Zn/Sn<1.0) with constant Cu content in precursors, produced Cu-rich and Sn-rich CZTS powder crystals. In the case of the highest Cu content in the precursors (Cu/(Zn+Sn) =1.1), additional phases of SnS, SnS<sub>2</sub>, and Sn<sub>2</sub>S<sub>3</sub> were detected by Raman and EDX analysis [10]. Several reports show that absorber materials growth in Cu-poor/Zn-rich conditions give the best solar cells efficiencies [22, 38–42].

G. Nkwusi *et al.* [39] described the chemical pathway of Cu<sub>2</sub>ZnSnS<sub>4</sub> synthesis in CdI<sub>2</sub> as follows:





or



CZTS formation goes through two stage process: first  $\text{Cu}_2\text{SnS}_3$  forms from  $\text{Cu}_2\text{S}$ ,  $\text{SnS}$  and  $\text{S}$ ; secondly  $\text{Cu}_2\text{SnS}_3$  reacts with  $\text{Zn}_{1-x}\text{Cd}_x\text{S}$  forming  $\text{Cu}_2\text{Zn}_{1-x}\text{Cd}_x\text{SnS}_4$ . However,  $\text{Cu}_2\text{Zn}_{1-x}\text{Cd}_x\text{SnS}_4$  can be directly formed from the binaries  $\text{Cu}_2\text{S}$ ,  $\text{SnS}$ ,  $\text{Zn}_{1-x}\text{Cd}_x\text{S}$  in the presence of sufficient amount of elemental sulfur.

### 1.2.2.3 Thermal treatment

Thermal treatment is applied to monograin powders after synthesis to modify their crystal surfaces which enhances the effectiveness of the working *p-n* junctions in monograin layer solar cells [4]. The treatment can be done in isothermal conditions or two-temperature zone and the operating conditions (temperature and pressure of treatment) of the thermal process can be easily controlled. Although the thermal treatment of kesterites takes place at temperatures as high as 740 °C, they have been reported to start decomposing at 400 °C [10]. The decomposition of quaternary compounds can be avoided during this process that involves high temperatures by keeping the sulfur pressure high and this prevents Sn losses, which in turn improves solar cell efficiency [48]. This can be achieved by the addition of  $\text{S}$  or  $\text{SnS}_2$  vapor as reported by M. Kauk *et al.* in their investigation of the effect of sulfur, selenium,  $\text{SnS}_2$  and  $\text{SnSe}_2$  vapor treatments on the elemental and phase composition of the monograins and on the properties of monograin layer (MGL) solar cells [48]. The monograin powder is heated in the higher temperature zone, while the elemental  $\text{S}$ ,  $\text{Se}$  or  $\text{SnS}_2$  and  $\text{SnSe}_2$  pellets are placed in the lower temperature zone which determines the vapor pressure of the components [4, 43]. The use of  $\text{SnS}$  in sulfurization treatment of CZTS nanocrystals has been reported to provide leverage with which to improve the compositional distribution of the final powder as well as the microstructure [49]. In CZTS thin films, increasing the annealing temperature to 550 °C improves the crystallinity of CZTS thin films, and reduces the number of secondary phases.

### 1.2.3 Defects of quaternary compounds

Cross-substituting binary building blocks can be used to form ternary and quaternary systems in a breeding process that can be used to tune the physicochemical properties such as bandgap and also keep properties such as the structure [45]. The presence of an additional element in the kesterite structure which accounts for the presence of three cations compared to the chalcopyrite structure, results in a larger number of possible intrinsic defects for CZTS and closely related compounds than for CIS [45, 46]. The presence of defects in a crystalline material may lead to local vibrational modes, which causes small additional features in the Raman spectra [46]. Grossberg *et al.* [52] proposed that the shoulder peak observed  $334.3\text{ cm}^{-1}$  during their Raman analysis of CZTS polycrystals can be attributed to the disordered kesterite. The kesterite (space group  $I4$ ) derived from the ternary chalcopyrite structure is the lowest energy structure of CZTS [12]. Figure 1.6 shows the tetragonal kesterite crystal structure of CZTS with corresponding cation ordering.

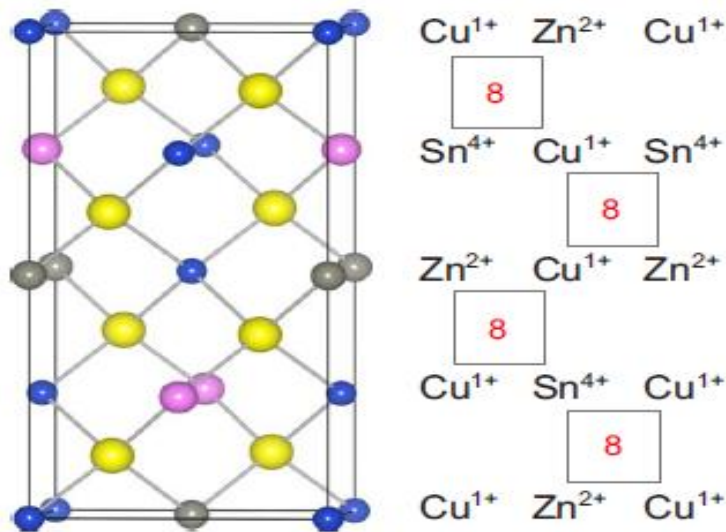


Figure 1.6 The tetragonal ( $I4$ ) kesterite crystal structure of CZTS (left) with the corresponding cation ordering (right) [40, 48].

An understanding of the thermodynamic stability of quaternary semiconductor compound CZTS and the formation mechanism of the dominant intrinsic defects is required to further improve the efficiency [40, 49]. In ternary compounds, the easy formation of the  $[2V_{\text{Cu}}^- + \text{In}_{\text{Cu}}^{2+}]$  defect complex is attributed to the presence of two cations, while in quaternary system CZTS, the

antisite defect pair  $[\text{Cu}_{\text{Zn}}^- + \text{Zn}_{\text{Cu}}^+]$  can be easily formed from three cations (Cu, Zn, and Sn) due to the smaller chemical and size disparities between the elements [45].

The defect structure of  $\text{Cu}_2\text{ZnSnS}_4$  (CZTS) material has been studied by Chen *et al.* [45] using theoretical electronic structure calculations. The presence of dominating self-compensated defect pair complexes such as  $[\text{V}_{\text{Cu}}^- + \text{Zn}_{\text{Cu}}^+]$  for Cu-poor/Zn-rich growth conditions and  $[\text{Cu}_{\text{Zn}}^- + \text{Zn}_{\text{Cu}}^+]$  for Cu-rich/Zn-poor condition was found in CZTS. This corroborates the earlier report of Nagoya *et al.* [54] from their theoretical studies. These defect complexes which are electrically neutral can remarkably passivate the deep levels in the bandgap, reducing the recombination in the PV device [4]. The authors' claim correlates with the report of other researchers that ZnS is the main competing phase under the prevalent Cu-poor and Zn-rich growth conditions, and Cu at Zn sites ( $\text{Cu}_{\text{Zn}}$ ) is the most stable defect in the entire stability range of CZTS [40, 46, 49, 50]. They further provided the following explanations to the unique features of CZTS:

- (i) The chemical potential region that CZTS can form stoichiometrically is very small [56]. Hence, to obtain high quality CZTS samples, the growth conditions must be controlled;
- (ii) The dominant *p*-type acceptor in CZTS is  $\text{Cu}_{\text{Zn}}$ , however, the associated acceptor level is relatively high, indicating that it is more demanding to have *p*-type doping in CZTS than in ternary compounds;
- (iii) The formation of the self-compensated defect pair  $[\text{Cu}_{\text{Zn}}^- + \text{Zn}_{\text{Cu}}^+]$  will not lead to strong carrier separation, and thus will not provide the same beneficial effect observed in ternary chalcopyrite compounds.

They predicted that growth under Cu-poor/Zn-rich conditions will yield optimal solar efficiency, as  $\text{V}_{\text{Cu}}$  and  $\text{Zn}_{\text{Cu}}$  become the dominant defects in the system which supports the report of other researchers [22, 38, 39, 48, 50].

#### **1.2.4 Metal ion substitution in $\text{Cu}_2\text{ZnSnS}_4$**

Metal ion substitution in monograin powder kesterite occurs amongst other ways, during the material synthesis because of the use of flux. CuSe-Se has been used as flux materials for the production of  $\text{CuInSe}_2$  monograins with nearly stoichiometric composition, however, the removal of the flux material after synthesis was difficult and this resulted in the use of potassium iodide (KI) which is water soluble [16]. The low melting point and water solubility of NaI and  $\text{CdI}_2$  also makes them to be good flux materials [10].

CIGS solar cells which have recorded admirable power conversion efficiency, have bandgap ( $E_g$ ) of 1.1-1.13 eV, which has yielded high efficiencies [58]. An ideal solar energy absorber material should have a bandgap around 1.3-1.4 eV, which is expected from Shockley-Queisser radiative limit (S-Q limit), and therefore the bandgap of solar cell absorber material needs to be adjusted to this energy region. In CZTS the bandgap adjustment should be at about 1.3-1.4 eV. It is possible to tune the composition of CZTS in other to achieve similar bandgap with CIGS. Jie Fu *et al.* suggested that the ideal way to reach this optimum bandgap level would be to reduce the S level by introducing some selenium in the synthesis process or by metal cation substitution process. In their work, they successfully incorporated about 5% of  $\text{Cd}^{2+}$  into the host lattice of CZTSSe to form a homogeneous  $\text{Cu}_2\text{Zn}_{1-x}\text{Cd}_x\text{Sn}(\text{S},\text{Se})_4$ , which improved the crystal growth process, lowered the band gap (1.12 eV) and improved the solar cell efficiency from 5.41 to 8.11% [59]. This result was also confirmed by Sun *et al.* [60] and Yan *et al.* [61] where the solar cell efficiency was increased from 5.3 to 9.8% and 8.8% to 11.5%, respectively. They have also reported several benefits of the metal cation substitution of Zn with Cd to form a solid solution of  $\text{Cu}_2(\text{Zn},\text{Cd})\text{SnS}_4$  (CZCdTS). Some of it included the reduction of ZnS secondary phase, and help to reduce the narrow single-phase region of CZTS. Balakrishna *et al.* also reported that the introduction of extrinsic impurities such as Fe and Mn (to replace Zn) or Se (to replace S) in the wurtzite structure of  $\text{Cu}_2\text{ZnSnS}_4$  resulted in variation of optical bandgap and microstructure of the thin films. They obtained the enhancement of the power conversion efficiency of a CZTS solar cell from 0.4% to 7.4% with selenium doping [24]. Most importantly, Nkwusi *et al.* reported the formation of  $\text{Cu}_2(\text{Zn},\text{Cd})\text{SnS}_4$  with about 3% of Cd incorporated into the solution of CZTS when synthesized in  $\text{CdI}_2$  at 780 °C [39], while Pilvet *et al.* reported the impact of Cd incorporation on the bandgap of the CZTS monograin powder materials [62].

### 1.2.5 Doping

Doping is the addition of the desired quantity of choice impurities to semiconductor crystals to alter their properties [60, 61]. The dopant (impurity) determines the type of doping by the number of outer electrons it possesses [63].

### 1.2.5.1 Effects of alkali metals doping to the solar cell absorber materials

The doping of CIGS, CIGSSe and CZTSSe with alkali metals have been reported by many researchers to enhance their photovoltaic performance [14, 24, 27, 62]. Grain size enlargement and improvement of surface morphology have been reported for doping CIGS,  $\text{Cu}_2\text{ZnSnSe}_4$  and  $\text{Cu}_2\text{ZnSn}(\text{S},\text{Se})_4$  film with Na [14, 63, 64]. Lopez-Marino *et al.* reported an increase in the efficiency of CZTSe thin film solar cells doped with Na from 2.2% to 4.3% and attributed the improvement to the higher  $V_{oc}$  and  $FF$  observed in the doped semiconductor [67]. Varying the concentration of Na in doping  $\text{CuInSe}_2$  monograin powder shows, that open circuit voltage increased until  $3 \times 10^{18} \text{ cm}^{-3}$  and decreased at higher concentrations. Sodium eliminates the  $\text{In}_{\text{Cu}}$  defects, thereby increasing the effective hole density [17]. According to the report of Klavina *et al.* in the study of  $\text{Cu}_2\text{ZnSnSe}_4$  monograin formation in molten KI, no new compound was formed in the  $\text{CuSe/KI}$ ,  $\text{ZnSe/KI}$  and  $\text{SnSe/KI}$  mixtures [15]. K-doping can enhance the preferred (112) orientation of CZTS thin films and also suppress secondary phases such as ZnS [14, 27]. Maeda *et al.* [65] reported from their investigations on the effect of potassium doping on CZTSSe using first-principles calculations, that K atoms cannot easily substitute for the Cu or Zn atoms in CZTS and CZTSe. They explained that this is because the covalent radius of K (1.96 Å) and its ionic radius (1.37 Å) are much larger than the covalent and ionic radius of Cu (1.27 Å/0.60 Å) and Zn (1.22 Å/0.60 Å), respectively. Tong *et al.* reported that K-doping in CZTS thin film resulted in reduction of open circuit voltage ( $V_{oc}$ ), increased short circuit current density ( $J_{sc}$ ), fill factor ( $FF$ ) and power conversion efficiency (PCE) [14]. They also showed that the doped CZTS has larger Raman peak intensity than the undoped semiconductor. Contrary to the report of Tong *et al.*, Hsieh *et al.* observed increase in  $V_{oc}$  for K-doped CZTSSe thin film, and also reported increase in  $J_{sc}$ ,  $FF$  and PCE [30].

## 1.3 Summary of literature review and objective of study

Currently, the best CZTS monograin layer solar cell showed conversion efficiency of 7.04% (active area 9.38%) [68]. In order to improve the efficiency of CZTS and achieve industrial production scale, the development of innovative technologies with higher conversion efficiencies and low production costs are an important. Cadmium ion substitution in CZTS has proven to be one of the ways to tune the band gap of CZTS to the optimum like that of CIGS which has

recorded high efficiencies and also to remove secondary phase of ZnS [11, 54]. Alkali metal doping of semiconductor absorber materials has also shown the ability to enhance PV characteristics [14, 27]. However, the concentration of the dopant has been reported to influence its impact on the photovoltaic characteristics of the solar cells from the doped absorber material [17, 69]. The focus of this work is to investigate the effect of potassium doping to the structural and optical properties of  $\text{Cu}_2(\text{Zn,Cd})\text{SnS}_4$  monograin powder, which is synthesized in cadmium iodide. Additionally, the aim was to find out the impact of K-doping on the  $\text{Cu}_2(\text{Zn,Cd})\text{SnS}_4$  monograin layer solar cells performances.

## 2. EXPERIMENTAL PROCEDURE

The steps involved in the preparation and characterization of monograin layer solar cells are described in this part. The  $\text{Cu}_2(\text{Zn,Cd})\text{SnS}_4$  powder used had already been grown by colleagues in our research group. The schematic in Figure 2.1 below shows the sequence of the experimental procedure and analysis.

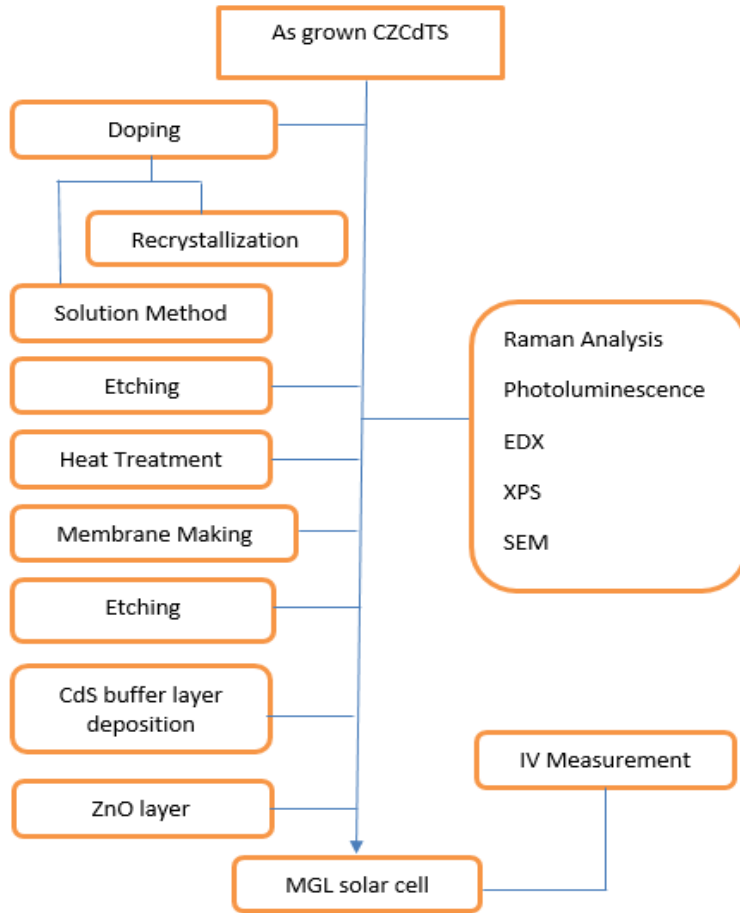


Figure 2.1. Sequence of experimental procedure and analysis

### 2.1 Preparation of $\text{Cu}_2(\text{Zn,Cd})\text{SnS}_4$ monograin layer solar cell

In this thesis, monograin powder was used as absorber material in the monograin layer solar cells, which has following structure: graphite/ $\text{Cu}_2(\text{Zn,Cd})\text{SnS}_4$ /CdS/i-ZnO/ZnO:Al. Following sections describe the technological steps for preparation of monograin layer solar cells.

### **2.1.1 Growth of monograin powders**

The  $\text{Cu}_2(\text{Zn,Cd})\text{SnS}_4$  powder used in the following experiments had already been grown by colleagues in our research group.  $\text{Cu}_2(\text{Zn,Cd})\text{SnS}_4$  monograin powder was synthesized from binary compounds (CuS, SnS and ZnS) and elemental S in  $\text{CdI}_2$  flux at  $740^\circ\text{C}$  for 120 hours. It is known that Cd from  $\text{CdI}_2$  flux incorporates to the crystals of  $\text{Cu}_2\text{ZnSnS}_4$  forming a solid solution of  $\text{Cu}_{2-x}\text{Zn}_x\text{Cd}_{1-x}\text{SnS}_4$  [39, 58].

### **2.1.2 Chemical etching**

After the synthesis of monograin powders, the first step involved the etching of the  $\text{Cu}_2(\text{Zn,Cd})\text{SnS}_4$  powder in 1%  $\text{Br}_2$  in methanol solution for 10 minutes. This was immediately followed by etching with 10% KOH in KCN solution for 10 minutes to achieve the desirable clean crystal surface and remove the secondary phases that may be present. After every etching stage, the powder samples were thoroughly rinsed with deionized water and then dried at  $50^\circ\text{C}$  after the final etching.

### **2.1.3 $\text{Cu}_2(\text{Zn,Cd})\text{SnS}_4$ doping with potassium**

In this study two methods were used for doping the  $\text{Cu}_2(\text{Zn,Cd})\text{SnS}_4$  monograin powders by potassium. In the first method was used an aqueous solution containing K as dopant. The second method was recrystallization of CZCdTS powder in KI flux. Latter method provides more homogeneous distribution of K, but it does not allow varying the concentration of potassium.

#### **2.1.3.1 K-doping from the solution**

For doping with K the chemically etched powder was subdivided into 6 portions and placed into the quartz vessels. The doping solution of KI as a source of K-dopant was added to each portion by varying the concentrations of K from  $1 \times 10^{16}$  to  $1 \times 10^{20}$  atoms per  $\text{cm}^3$  of CZCdTS. The last portion was not doped, this was kept as reference powder to ensure we can determine the impact of doping on the other samples.

Following calculations show the procedure how the doping concentrations were determined.

$$\text{Initial concentration (C)} = 1 \times 10^{20} \text{ atoms/cm}^3$$

Molar mass of KI (M) = 166 g/mol

Avogadro constant ( $N_A$ ) =  $6.02 \times 10^{23}$  atoms/mol

Volume of solution (V) =  $10 \text{ cm}^3$

$$\begin{aligned} C \text{ in } \frac{\text{mol}}{\text{dm}^3} &= 1 \times 10^{20} \frac{\text{atoms}}{\text{cm}^3} \div 6.02 \times \frac{10^{23} \text{atoms}}{\text{mol}} \\ &= 1.66 \times 10^{-4} \text{mol/cm}^3 \\ &= 0.166 \text{mol/dm}^3 \end{aligned}$$

Mass (m) of KI required to make a solution with concentration of  $0.166 \text{ mol/dm}^3$  ( $1 \times 10^{20}$  atoms/cm<sup>3</sup>) in  $10 \text{ cm}^3$  solution is calculated below.

$$\begin{aligned} m &= M \times C \times V \div 1000 \text{cm}^3 \\ &= \frac{166 \text{g}}{\text{mol}} \times \frac{0.166 \text{mol}}{\text{dm}^3} \times 10 \text{cm}^3 \div 1000 \text{cm}^3 \\ &= 0.276 \text{g} \end{aligned}$$

The powders were desiccated in thermostat at  $50 \text{ }^\circ\text{C}$  for 24 hours. The dried powders were sealed in quartz ampoules and annealed at  $740 \text{ }^\circ\text{C}$  in sulfur vapor ( $p_S = 1000 \text{ Torr}$  at  $465 \text{ }^\circ\text{C}$ ) by using two temperature zone furnace. The annealed samples were sieved to narrow fractions to ensure the uniformity of grain size for preparation of monograin layer solar cell. All membranes were done by Dr. Tiit Varema who works in our research group.

### 2.1.3.2 Doping by recrystallization method

The K-doping of the CZCdTS was done by recrystallization in KI flux. This was achieved by adding equal mass of potassium iodide to 1.64 g of CZCdTS powder in fraction 63-90  $\mu\text{m}$ . The mixture was sealed in quartz ampoule and annealed at elevated temperature. The reaction temperature was set at  $720 \text{ }^\circ\text{C}$ , which is above the melting point of potassium iodide ( $T_m = 686 \text{ }^\circ\text{C}$ ). The process was carried out for a duration of 108 hours. After annealing, the ampoule was quenched to room temperature and flux was removed by DI-H<sub>2</sub>O. After drying, the powder was

sieved to 3 different fractions: 63-75  $\mu\text{m}$ , 75-80  $\mu\text{m}$  and 80-90  $\mu\text{m}$ . Monograin layer solar cells were made from crystals with size 63-75  $\mu\text{m}$ .

#### 2.1.4 Buffer layer by Chemical Bath Deposition

*p-n* junction is form by depositing *n*-type CdS thin layer on *p*-type CZCdTS monograin layer (MGL) membrane. Before the chemical deposition of CdS, the membranes were etched with bromine in methanol solution followed by treatment with potassium cyanide to activate the surface. The membranes were rinsed with deionized water and dried with nitrogen flow after each etching step. The chemical bath deposition was conducted immediately after activating the surface of the cells through etching. The MGL membranes were placed in the chemical bath deposition (CBD) solution (see Figure 2.2), and allowed for CdS layer deposition for a duration of 20 minutes at 45 °C to get buffer layer thickness of  $\square 30$  nm.

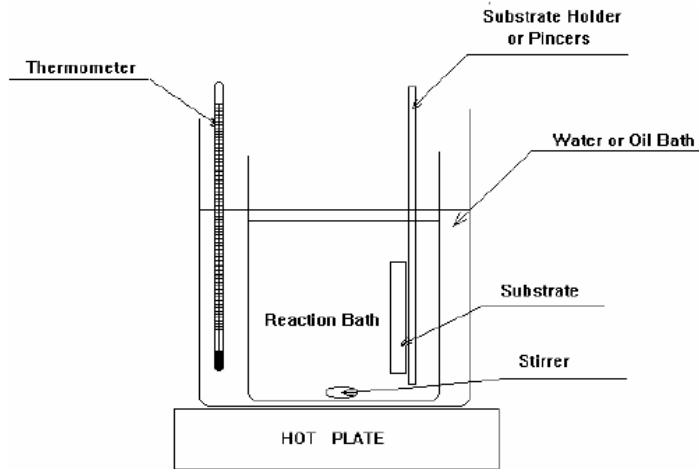


Figure 2.2. Chemical bath deposition set up [36].

Predetermined quantities of precursor solutions were mixed together to achieve the working aqueous solution. The precursor solutions for cadmium sulfide deposition contain: DI water, CdI<sub>2</sub> (0.01M), NH<sub>4</sub>OH (2M) and TU (1M). The respective quantities used for CdS deposition are brought in Table 2.1. Except of TU, which was the last to be added, all the other precursor solutions were placed in a reagent bottle in the sequence stated above and mixed together. Table 2.1 shows the quantities of each precursor used in making the aqueous solution for the chemical bath deposition.

Table 2.1 Precursor solution for CdS.

Precursor solutions	Concentration of precursor solution, [mol/L]	Volume to make 150 ml of solution, [ml]	Conc. in deposition solution, [mol/L]
H <sub>2</sub> O		29.25	
CdI <sub>2</sub>	0.01	21	0.0014
NH <sub>4</sub> OH	2	78.75	1.05
TU (SC(NH <sub>2</sub> ) <sub>2</sub> )	1	21	0.14

The membranes were rinsed with deionized water after the CdS buffer layer deposition and then annealed at 160 °C in the thermostat for 10 minutes.

### 2.1.5 Window layer deposition and formation of back contacts

The i-ZnO/ZnO:Al window double layer was then deposited by radio-frequency (RF) sputtering. Thereafter, silver (Ag) paste was used to create contact on the membranes before being glued to glass using epoxy to give it the required strength. Upon drying, the substrate foils on the back side of the membranes were removed before etching with concentrated sulfuric acid for 50 seconds to remove the leftover epoxy on the cell membranes. The etched crystals were then mechanically polished with sandpaper before applying the graphite back contact. Characterization of the completed cells was conducted afterward using current-voltage (*I-V*) measurements.

## 2.2 Characterization of monograins and solar cells

The monograin powders and solar cells were characterized using different methods of analysis as stated in Table 2.2.

Table 2.2 Characterization techniques and equipment used.

Properties	Analytical method	Operator
Morphology	Scanning electron microscope (SEM)	Dr. Valdek Mikli
Bulk composition	Energy dispersive x-ray spectroscopy (EDX)	Dr. Valdek Mikli
Surface composition	X-ray photoelectron spectroscopy (XPS)	Dr. Mati Danilson
Phase composition	Raman spectroscopy (RAMAN)	Adekunle I. Lasisi
Optical properties	Photoluminescence (PL)	Dr. Maarja Grossberg
Solar cell characteristics	Current density-voltage measurement ( <i>I-V</i> )	Adekunle I. Lasisi

### 2.2.1 Current-voltage characteristics of solar cells

The output parameters of MGL solar cells were deduced from  $I$ - $V$  characteristics. The most important solar cell parameters obtained from  $I$ - $V$  measurements are short-circuit current density ( $J_{sc}$ ), open-circuit voltage ( $V_{oc}$ ), fill factor ( $FF$ ) and the solar energy conversion efficiency  $\eta$ . The solar energy conversion efficiency  $\eta$  of the cell is the ratio of the maximum power (electrical) density delivered by the cell to the power density from the reference light source. The efficiency can be represented by Eq. 2.1 below:

$$\eta = \frac{j_{sc} \times V_{oc} \times FF}{P_{in}} \quad (2.1)$$

where  $\eta$  - efficiency;

$j_{sc}$  - short circuit current density;

$V_{oc}$  - open circuit voltage;

$FF$  - fill factor;

$P_{in}$  - power of the standard illumination (100 mW/cm<sup>2</sup>) used.

The fill factor of the solar cell, which can be used to describe the quality of the solar cell junction, can be calculated by Eq. 2.2:

$$FF = \frac{j_{eff} \times V_{eff}}{j_{sc} \times V_{oc}} \quad (2.2)$$

where  $FF$  - fill factor;

$j_{eff}$  - current density at maximum power output;

$V_{eff}$  - voltage at maximum power output;

$V_{oc}$  - open circuit voltage;

$j_{sc}$  - short circuit current density.

### 3. RESULTS AND DISCUSSION

#### 3.1 Elemental composition

##### 3.1.1 Composition of $\text{Cu}_2\text{Zn}_{1-x}\text{Cd}_x\text{SnS}_4$ crystals synthesized in $\text{CdI}_2$ flux

The chemical composition of synthesized  $\text{Cu}_2\text{Zn}_{1-x}\text{Cd}_x\text{SnS}_4$  monograin powders was analyzed by energy dispersive X-ray spectroscopy. Initial compositional ratios of precursor mixture were  $\text{Cu}/\text{Sn} = 1.8$  and  $\text{Zn}/\text{Sn} = 1.0$ . Bulk compositional analyses by EDX were made from polished cross-section of individual crystals of  $\text{Cu}_2\text{Zn}_{1-x}\text{Cd}_x\text{SnS}_4$  powders as seen in Figure 3.1 and presented in Table 3.1. Results show that the ratio of  $\text{Cu}/\text{Sn}$  is increased from 1.8 in precursor mixture to 2.09 in outcome powder. EDX analysis showed that Zn is substituted by Cd about 14% in  $\text{Cu}_2\text{ZnSnS}_4$  lattice forming the solid solution with chemical formula  $\text{Cu}_{2.09}(\text{Zn}_{0.86}\text{Cd}_{0.14})_{1.13}\text{SnS}_{4.22}$ .

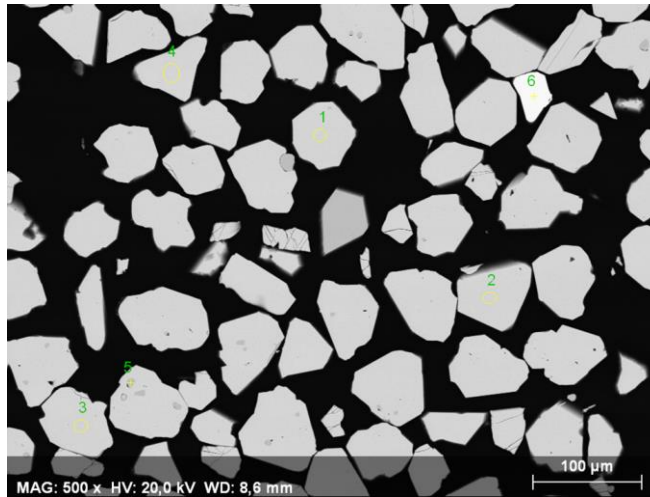


Figure 3.1. SEM image of polished cross-section of individual crystals of  $\text{Cu}_2\text{Zn}_{1-x}\text{Cd}_x\text{SnS}_4$  powder.

Table 3.1. Composition of  $\text{Cu}_2\text{ZnSnS}_4$  powder synthesized in  $\text{CdI}_2$  flux.

	Elemental composition					Compositional ratios of synthesized powder			
	Cu, at%	Zn, at%	Cd, at%	Sn, at%	S, at%	$\frac{[\text{Cu}]}{([\text{Zn}]+[\text{Cd}]+[\text{Sn}] )}$	$\frac{[\text{Cu}]}{[\text{Sn}]}$	$\frac{[\text{Cd}]}{([\text{Cd}]+[\text{Zn}])}$	$\frac{([\text{Cd}]+[\text{Zn}])}{[\text{Sn}]}$
Objects 1	24.74	11.59	1.95	11.89	49.83	0.97	2.08	0.14	1.14
Objects 2	24.96	11.67	1.95	11.67	49.75	0.99	2.14	0.14	1.17
Objects 3	24.79	11.36	1.91	11.86	50.07	0.99	2.09	0.14	1.12
Objects 4	24.51	11.35	1.92	11.94	50.27	0.97	2.05	0.14	1.11
<b>Average</b>	<b>24.75</b>	<b>11.49</b>	<b>1.93</b>	<b>11.84</b>	<b>49.98</b>	<b>0.98</b>	<b>2.09</b>	<b>0.14</b>	<b>1.13</b>

### 3.1.2 Composition of $\text{Cu}_2\text{Zn}_{1-x}\text{Cd}_x\text{SnS}_4$ crystals recrystallized in KI flux

The chemical composition of recrystallized  $\text{Cu}_2\text{Zn}_{1-x}\text{Cd}_x\text{SnS}_4$  monograin powder in KI was also analyzed by energy dispersive X-ray spectroscopy (EDX). Table 3.2 shows elemental composition and compositional ratios in recrystallized powder. Compositional analysis showed that atomic content of elements did not change after recrystallization in KI. It means that powder composition remained the same in bulk after recrystallization in KI.

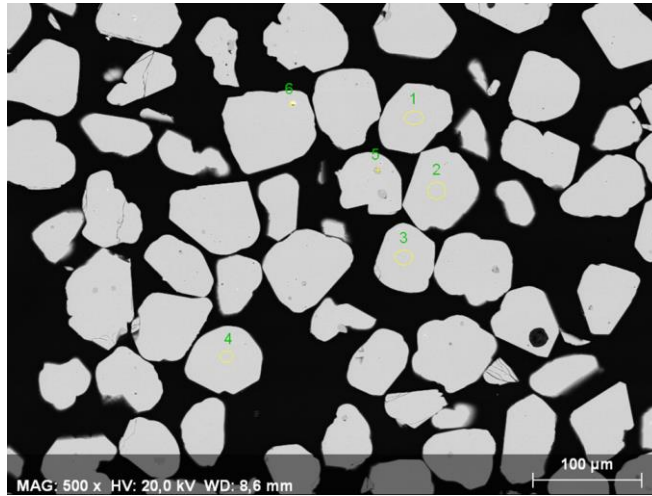


Figure 3.2. SEM image of polished cross-section of individual crystals of  $\text{Cu}_2\text{Zn}_{1-x}\text{Cd}_x\text{SnS}_4$  powder after recrystallization in KI.

Table 3.2. Composition of  $\text{Cu}_2\text{Zn}_{1-x}\text{Cd}_x\text{SnS}_4$  crystals recrystallized in KI flux

	Elemental composition					Compositional ratios of synthesized powder			
	Cu, at%	Zn, at%	Cd, at%	Sn, at%	S, at%	$\frac{[\text{Cu}]}{([\text{Zn}]+[\text{Cd}]+[\text{Sn}] )}$	$\frac{[\text{Cu}]}{[\text{Sn}]}$	$\frac{[\text{Cd}]}{([\text{Cd}]+[\text{Zn}])}$	$\frac{([\text{Cd}]+[\text{Zn}])}{[\text{Sn}]}$
Objects 1	24.64	11.46	1.87	11.79	50.24	0.98	2.09	0.14	1.13
Objects 2	24.59	11.63	1.94	11.74	50.11	0.97	2.09	0.14	1.16
Objects 3	24.81	11.46	1.92	11.87	49.94	0.98	2.09	0.14	1.13
Objects 4	24.73	11.53	1.90	12.06	49.79	0.97	2.05	0.14	1.11
<b>Average</b>	<b>24.69</b>	<b>11.52</b>	<b>1.91</b>	<b>11.87</b>	<b>50.02</b>	<b>0.98</b>	<b>2.08</b>	<b>0.14</b>	<b>1.13</b>

The compositional ratio of  $\frac{[\text{Cu}]}{([\text{Zn}]+[\text{Cd}]+[\text{Sn}])} = 0.98$  and  $\frac{([\text{Cd}]+[\text{Zn}])}{[\text{Sn}]} = 1.13$ , indicates that the monograin powder is synthesized under Cu-poor and (Zn+Cd)-rich conditions, which has been reported in literature as the best condition to get the most efficient solar cells [40, 46, 49, 50]. The compositional ratio of  $\frac{([\text{Cd}]+[\text{Zn}])}{[\text{Sn}]} = 1.13$ , indicates that monograin powder is (Zn, Cd)-rich. Additionally to  $\text{Cu}_2\text{Zn}_{1-x}\text{Cd}_x\text{SnS}_4$  phase, (Zn,Cd)S secondary phase was also observed

(see Figure 3.1 and Figure 3.2 marked by point 5). These dark areas inside the crystals had elemental composition Zn 45.9 at%, Cd 4.1 at% and S 49.9 at%.

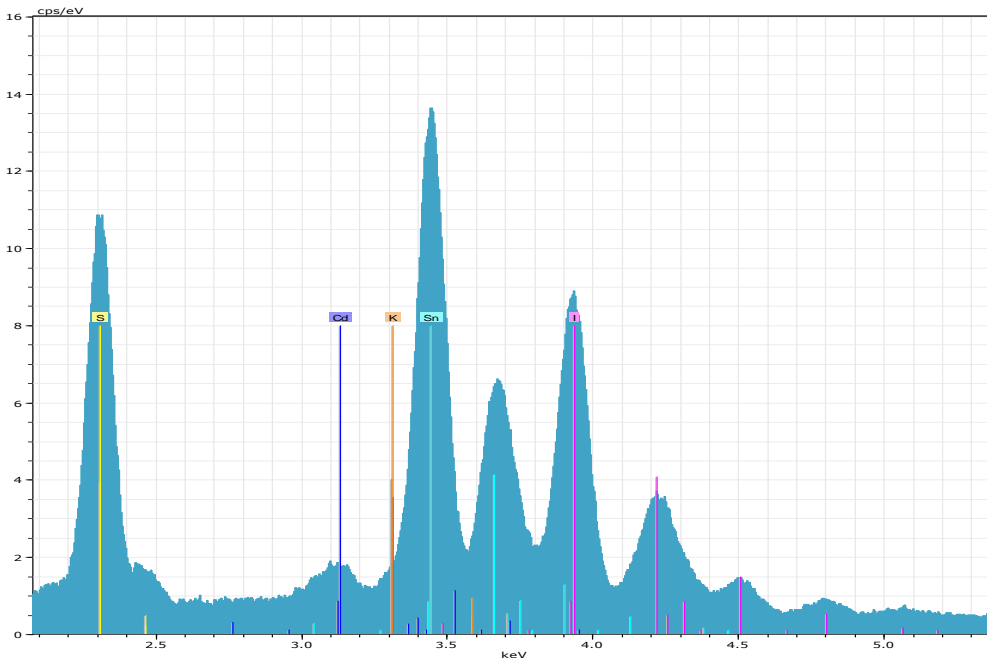


Figure 3.3 Energy dispersive X-ray analysis spectrum of  $\text{Cu}_2\text{Zn}_{1-x}\text{Cd}_x\text{SnS}_4$  crystal surface.

Figure 3.3 presents part of the EDX spectrum of  $\text{Cu}_2\text{Zn}_{1-x}\text{Cd}_x\text{SnS}_4$  crystal surface. Due to overlapping of Sn and K peaks in EDX spectrum, it is very difficult to distinguish K and Sn and calculate elemental concentrations. Therefore, to determine the concentration of K on the surface of  $\text{Cu}_2\text{Zn}_{1-x}\text{Cd}_x\text{SnS}_4$ , more precise analytic method should be used. One possible method for that is X-ray photoelectron spectroscopy (XPS). XPS is very sensitive to the chemical composition and environment of the elements in a material.

### 3.1.3 Surface composition by XPS

As the dopant concentration was below the measurement limit of EDX analysis, the surface composition of both the undoped and the doped (recrystallized) powder were analyzed by X-ray photoelectron spectroscopy (XPS). Figure 3.4 shows XPS survey spectra (0– 1200 eV) of undoped and K- doped  $\text{Cu}_2\text{Zn}_{1-x}\text{Cd}_x\text{SnS}_4$  powders. According to the XPS spectra the expected valence states of all the elements in the solid solutions of CZCdTS are confirmed. The core level peaks corresponding to the elements copper (Cu 2p), zinc (Zn 2p), tin (Sn 3d), cadmium (Cd 3p)

and sulfur (S 2p) can be visibly seen in the spectra. In addition, it also shows the presence of I 3d peaks in undoped powder surface and K 2s and 2p peaks in doped crystals surface, respectively as impurities.

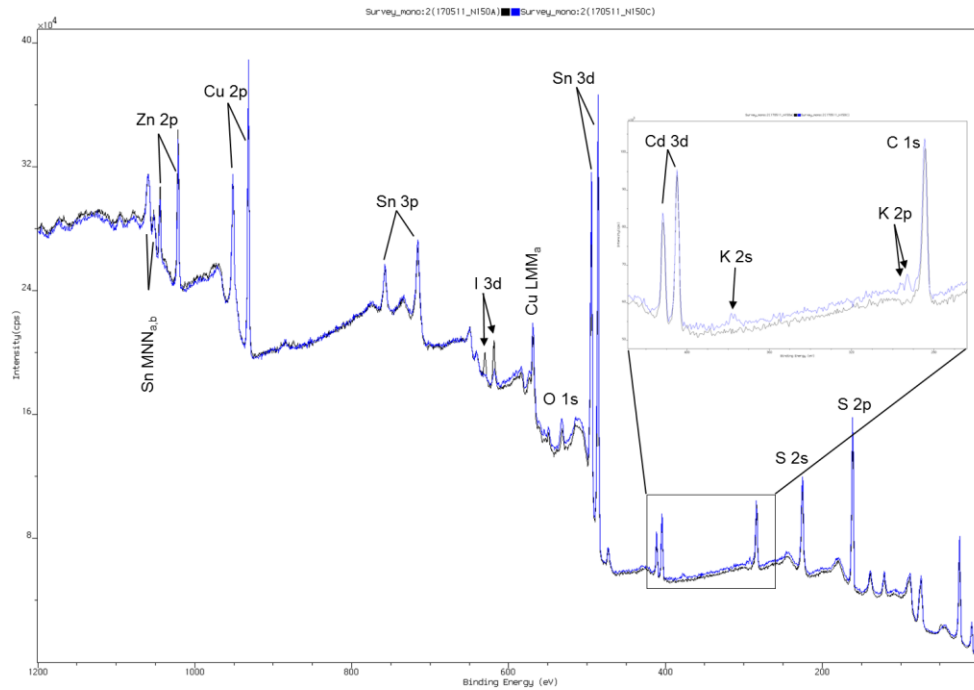


Figure 3.4. XPS analysis of surface composition of undoped (black curve) and K-doped (blue curve) crystals.

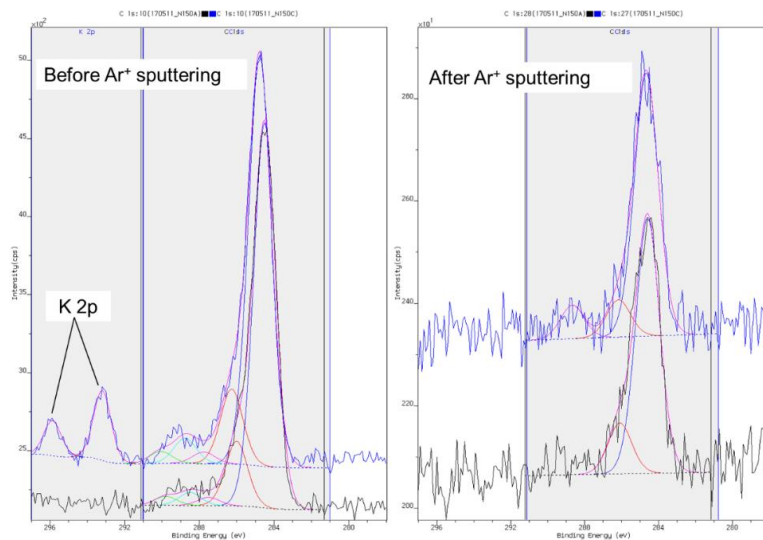


Figure 3.5. K 2p spectra of  $\text{Cu}_2\text{Zn}_{1-x}\text{Cd}_x\text{SnS}_4$  powder before and after  $\text{Ar}^+$  sputtering.

Figure 3.5 shows high-resolution XPS spectrum of K 2p consisting two peaks at 293.2 and 296.0eV, which disappear after  $\text{Ar}^+$  sputtering. This is the evidence that K incorporation to  $\text{Cu}_2\text{Zn}_{1-x}\text{Cd}_x\text{SnS}_4$  powder is only on the surface layer.

Table 3.3. The Zn, Cd, K and I content in  $\text{Cu}_2\text{Zn}_{1-x}\text{Cd}_x\text{SnS}_4$  powder surface by XPS

Samples	Zn (at. %)	Cd (at. %)	I (at. %)	K (at. %)	$[\text{Cd}]/([\text{Cd}]+[\text{Zn}])$
$\text{Cu}_2\text{Zn}_{1-x}\text{Cd}_x\text{SnS}_4-\text{CdI}_2$	9.34	1.61	0.83	-	0.16
$\text{Cu}_2\text{Zn}_{1-x}\text{Cd}_x\text{SnS}_4-\text{KI}$	9.64	2.04	-	0.98	0.17

Elemental composition of undoped and K-doped  $\text{Cu}_2\text{Zn}_{1-x}\text{Cd}_x\text{SnS}_4$  powder surfaces by XPS are presented in Table 3.3. In comparison to the EDX analysis from bulk  $\text{Cu}_2\text{Zn}_{1-x}\text{Cd}_x\text{SnS}_4$  crystals, the concentration of Zn is decreased on the surface in both powders, but  $\text{Cu}_2\text{Zn}_{1-x}\text{Cd}_x\text{SnS}_4$  powder synthesized in  $\text{CdI}_2$  has lower Cd content on the surface than in bulk. After recrystallizations in KI, the content of Cd is increased compared to bulk analysis by EDX. The ratio of  $[\text{Cd}]/([\text{Cd}]+[\text{Zn}])$  shows that Zn substitution by Cd in the surface is increased from 14 % to 16-17%. According to XPS analysis, the surface of  $\text{Cu}_2\text{Zn}_{1-x}\text{Cd}_x\text{SnS}_4$  powder after recrystallization in KI contain ~1 at% potassium.

## 3.2 Structural study of K-doped $\text{Cu}_2\text{Zn}_{1-x}\text{Cd}_x\text{SnS}_4$ monograin powders

### 3.2.1 Raman spectroscopy analysis

Raman spectroscopy study is useful to investigate the phase purity and composition of kesterite materials. Figure 3.6 shows Raman spectra of  $\text{Cu}_2\text{Zn}_{1-x}\text{Cd}_x\text{SnS}_4$  synthesized in  $\text{CdI}_2$  after K-doping from solution.

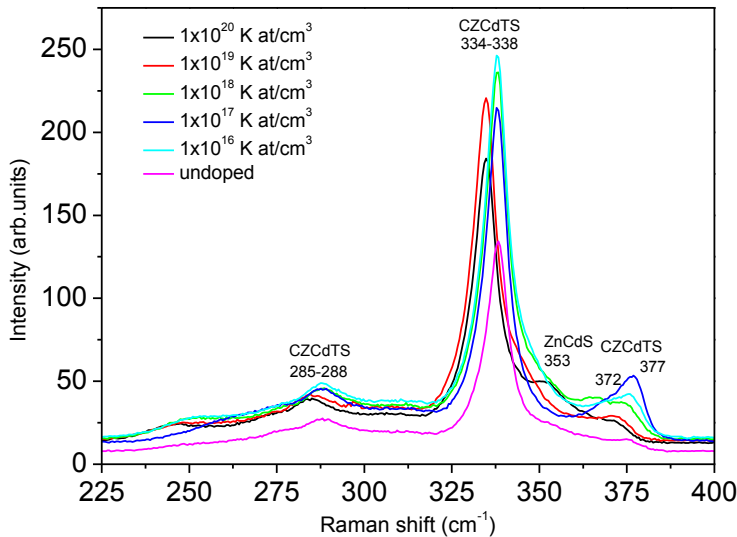


Figure 3.6. Raman spectra of  $\text{Cu}_2\text{Zn}_{1-x}\text{Cd}_x\text{SnS}_4$  synthesized in  $\text{CdI}_2$  with different concentration of K from solution.

The characteristic Raman frequencies of  $\text{Cu}_2\text{Zn}_{1-x}\text{Cd}_x\text{SnS}_4$  are at 286, 335 and 375  $\text{cm}^{-1}$  [28, 39, 70]. It was observed that the undoped monograin powder has the lowest intensity compared to the doped monograin powders and this is consistent with the report of Tong *et al* [14]. An additional (Zn,Cd)S secondary phase with characteristic Raman mode at 353  $\text{cm}^{-1}$  was detected. The presence of (Zn,Cd)S phase in the material was supported also by the results of EDX analysis. Raman spectra of  $\text{Cu}_2\text{Zn}_{1-x}\text{Cd}_x\text{SnS}_4$  synthesized in  $\text{CdI}_2$  and  $\text{Cu}_2\text{Zn}_{1-x}\text{Cd}_x\text{SnS}_4$  monograin powder crystals after recrystallisation in KI are presented in Figure 3.7. Similar peak positions at 286, 337 and 377  $\text{cm}^{-1}$  are observed for both the undoped and doped crystals just as in the case of the solution doped crystals.

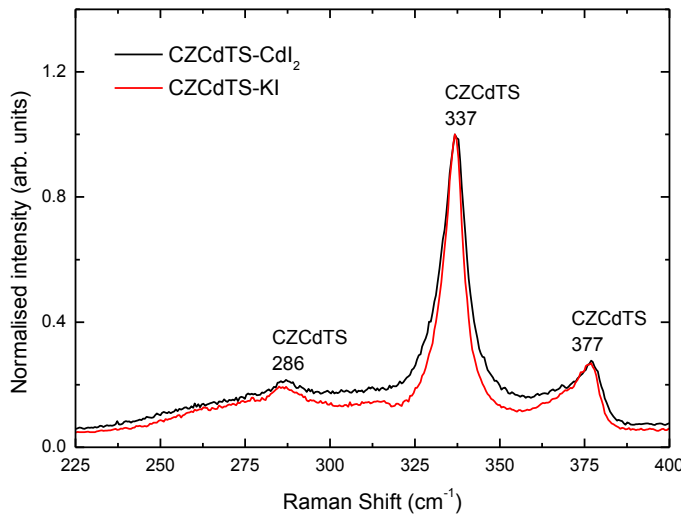


Figure 3.7. Raman spectra of  $\text{Cu}_2\text{Zn}_{1-x}\text{Cd}_x\text{SnS}_4$  synthesized in  $\text{CdI}_2$  and  $\text{Cu}_2\text{Zn}_{1-x}\text{Cd}_x\text{SnS}_4$  monograin powder crystals after recrystallisation in KI.

### 3.3 Morphology of $\text{Cu}_2\text{Zn}_{1-x}\text{Cd}_x\text{SnS}_4$ monograin powder crystals

The shape and surface morphology of crystals were studied with the high resolution scanning electron microscope (SEM). As observed in Figure 3.8, crystals of the undoped powder synthesized in cadmium iodide (A-B) have sharp edges compared to the monograin powder crystals recrystallized in KI (C-D) which have smooth edges. Also, the crystals of the powder recrystallized in KI have a brighter appearance than the undoped crystals.

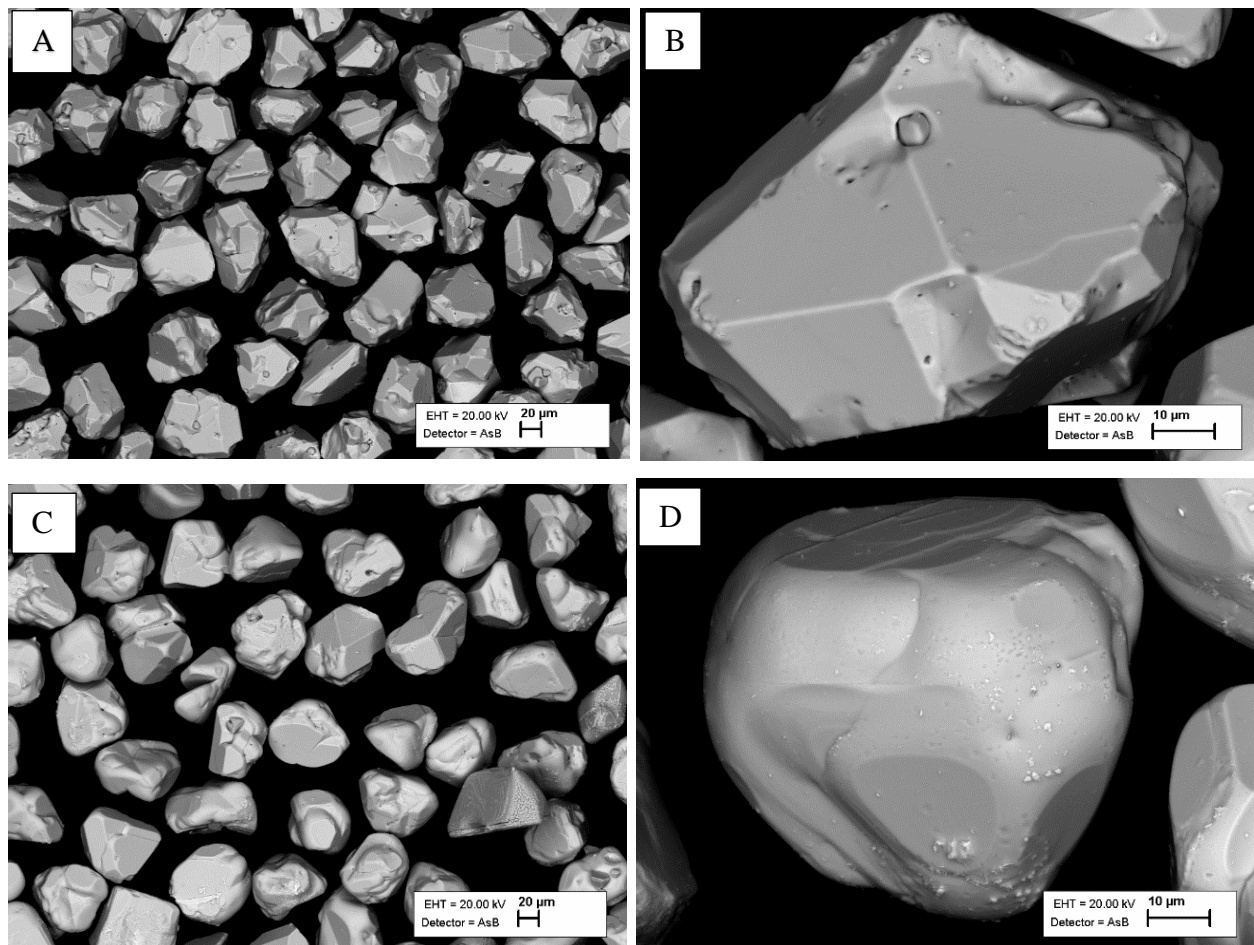


Figure 3.8. SEM micrographs of  $\text{Cu}_2\text{Zn}_{1-x}\text{Cd}_x\text{SnS}_4$  monograin powder synthesized in  $\text{CdI}_2$  flux (left) and the recrystallized monograin powder (right).

### 3.4 Photoluminescence study

Optical properties are characterized by low-temperature ( $T=10$  K) PL measurements. Normalized PL spectra of  $\text{Cu}_2\text{Zn}_{1-x}\text{Cd}_x\text{SnS}_4$  monograin powders with different concentration of K added from solution are presented in Figure 3.9. Low-temperature PL spectra are consisted of one broad asymmetric PL band at 1.18 eV for all powders. PL bands with such an asymmetric shape are often observed in multinary compounds that contain large concentrations of charged defects [71].

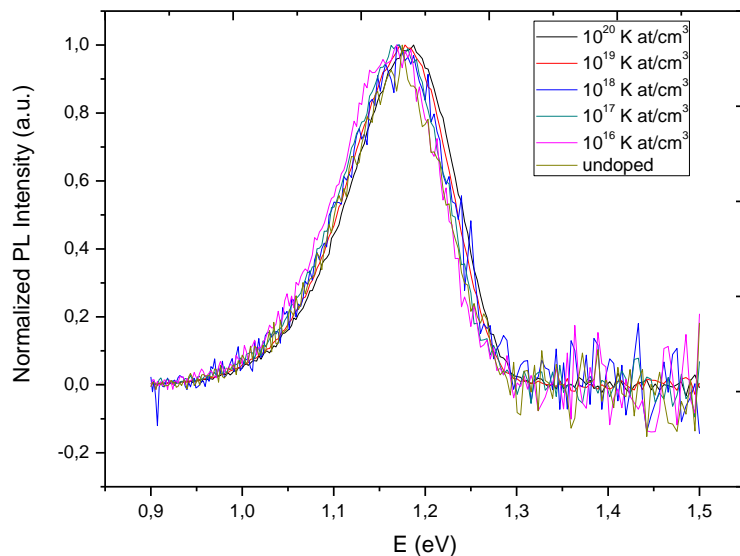


Figure 3.9. Normalized low-temperature PL spectra of the K-doped  $\text{Cu}_2\text{Zn}_{1-x}\text{Cd}_x\text{SnS}_4$  monograin powders.

As seen from Figure 3.10, the intensity of PL spectra increases about 8 times with addition of K, but no shift of PL band position was observed by K-doping from solution.

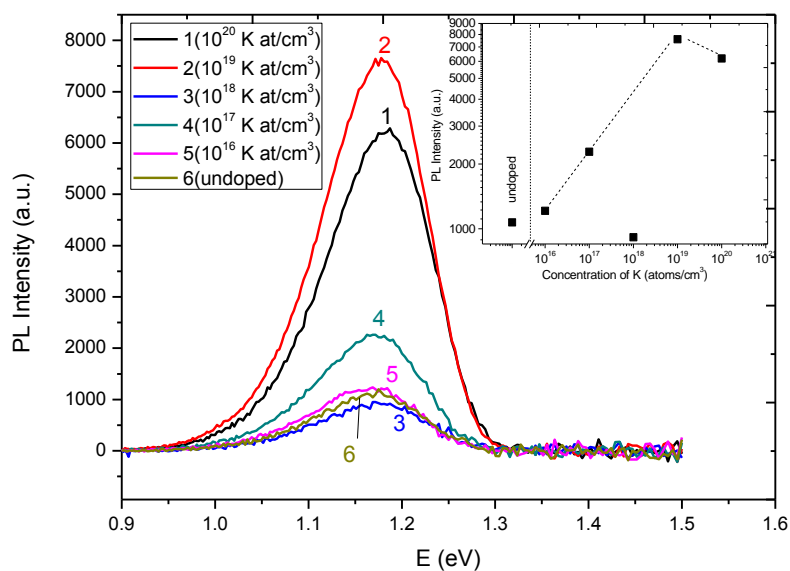


Figure 3.10. Low-temperature PL spectra of the  $\text{Cu}_2\text{Zn}_{1-x}\text{Cd}_x\text{SnS}_4$  monograin powders with different concentration of K (inset graph shows PL band intensity depending on the added K concentration).

Room-temperature PL spectra of the  $\text{Cu}_2\text{Zn}_{1-x}\text{Cd}_x\text{SnS}_4$  monograin powders synthesised in  $\text{CdI}_2$  and recrystallised in KI are presented in Figure 3.11. Both spectra are consisted of one broad asymmetric PL band at 1.45 eV in  $\text{Cu}_2\text{Zn}_{1-x}\text{Cd}_x\text{SnS}_4$  - $\text{CdI}_2$  and 1.4 eV in  $\text{Cu}_2\text{Zn}_{1-x}\text{Cd}_x\text{SnS}_4$  -KI, respectively. The shift of the PL band position (see Figure 3.11a) could be caused by different cooling process after the growth of powders. Timmo *et al.* [72] found that different rate of cooling causes the cation disordering in crystal structure. Figure 3.11b shows that intensity of PL band increased after recrystallization in KI. This is in good correlation with PL results of K-doping from solution studies.

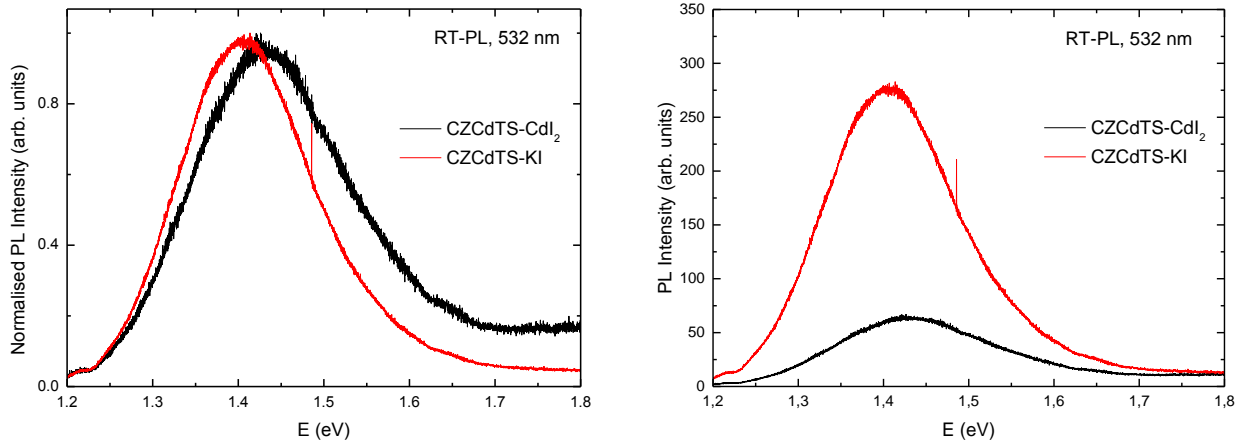


Figure 3.11. Room-temperature PL spectra of the  $\text{Cu}_2\text{Zn}_{1-x}\text{Cd}_x\text{SnS}_4$  monograin powders synthesised in  $\text{CdI}_2$  and recrystallized in KI (right graph is normalized and left is not).

### 3.5 Device characterization

$\text{Cu}_2\text{Zn}_{1-x}\text{Cd}_x\text{SnS}_4$  solar cells parameters based on monograin powders with variable concentration of potassium added from solution are presented in Figure 3.12 and Figure 3.13. The increase in  $V_{oc}$  with doping is consistent with some reports in literature [27, 67], but is contrary to the report of Tong *et al.* in which  $V_{oc}$  reduced as the concentration of K increased in the CZTS thin films [14]. However,  $V_{oc}$  gradually decreased at the peak concentrations. The value of short circuit current density increased by K-doping in concentration up to  $10^{19}$   $\text{at}/\text{cm}^3$ , the subsequent addition of potassium was detrimental to all output parameters. This is quite similar to the reports of  $J_{sc}$  increasing with carrier concentration in Na doping [17, 69]. Adding K in concentration  $10^{19}$   $\text{at}/\text{cm}^3$  yielded the highest power conversion efficiency of 3.52%.

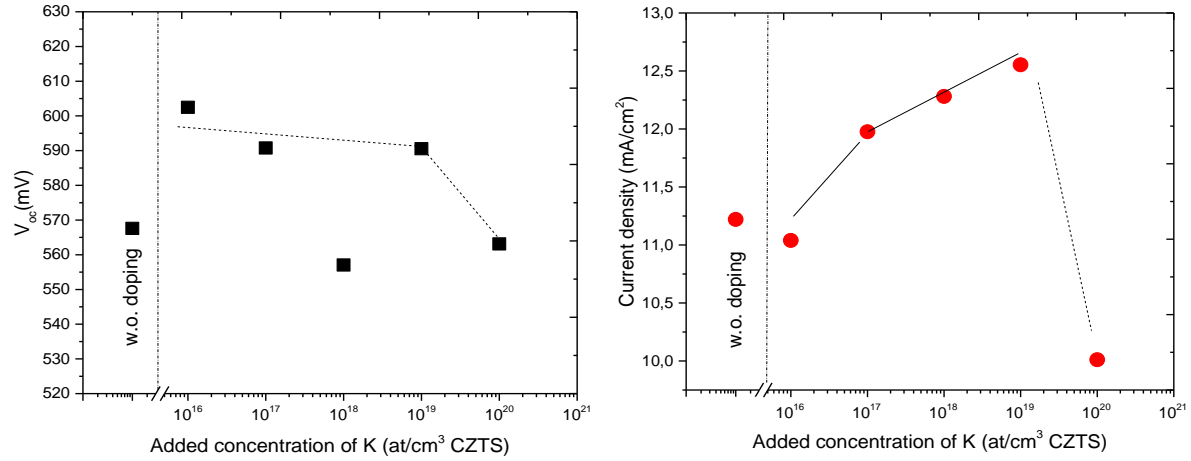


Figure 3.12. Influence of varying concentration of K in monograin powder on open circuit voltage and short circuit current density.

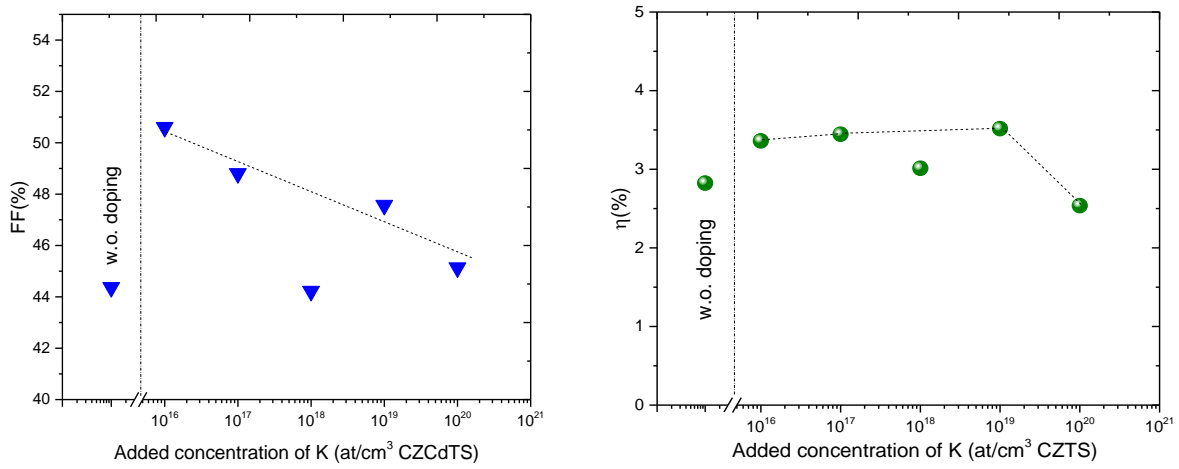


Figure 3.13. Influence of varying concentration of K in monograin powder on fill factor and power conversion efficiency.

It was observed that the  $I$ - $V$  characteristics of the cell made from monograin powder doped with concentration of  $10^{18}$  at/cm<sup>3</sup> KI solution deviates from the regular pattern observed in other cells. This is due to the inconsistency in the mechanical processes involved in the making of the solar cell. All output parameters of monograin layer solar cells based on K-doped  $\text{Cu}_2\text{Zn}_{1-x}\text{Cd}_x\text{SnS}_4$  powders are listed in Table 3.4.

Table 3.4. Output parameters of monograin layer solar cells based on undoped and K-doped  $\text{Cu}_2\text{Zn}_{1-x}\text{Cd}_x\text{SnS}_4$  powders.

Samples	V <sub>OC</sub> (mV)	FF (%)	J (mA/cm <sup>2</sup> )	η (%)
Undoped	567	41.8	11.2	2.8
10 <sup>16</sup>	602	50.6	11.0	3.4
10 <sup>17</sup>	591	48.8	12.0	3.5

$10^{18}$	557	44.2	12.3	3.0
$10^{19}$	591	47.6	12.6	3.5
$10^{20}$	563	45.2	10.0	2.5

According to XPS results, the K-containing surface layer is very thin after recrystallization. Therefore, the monograin layer solar cells were prepared by using two pre-treatments methods for  $\text{Cu}_2\text{Zn}_{1-x}\text{Cd}_x\text{SnS}_4$  powders: a) standard technology step- chemical etching with 1% Br in MeOH solution followed by KCN solution before post-treatment in sulfur vapor at 740 °C and b) without chemical etching followed by annealing in sulfur vapor at 740 °C.

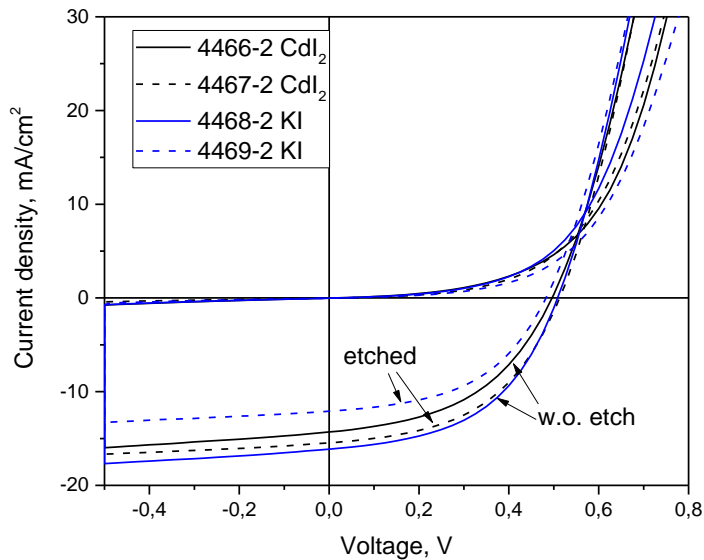


Figure 3.14 The  $I$ - $V$  characteristics of the solar cells based on  $\text{Cu}_2\text{Zn}_{1-x}\text{Cd}_x\text{SnS}_4$  monograin powders synthesized in  $\text{CdI}_2$  and recrystallized in KI with and without chemical etching before sulfurization.

The  $I$ - $V$  characteristics of the solar cells from  $\text{Cu}_2\text{Zn}_{1-x}\text{Cd}_x\text{SnS}_4$  monograin powder grown in  $\text{CdI}_2$  flux and from  $\text{Cu}_2\text{Zn}_{1-x}\text{Cd}_x\text{SnS}_4$  monograin powder recrystallized in KI with and without chemical etching before post-treatment in sulfur vapor are presented in Figure 3.14. In Table 3.5 are presented all output parameters for solar cells based on  $\text{Cu}_2\text{Zn}_{1-x}\text{Cd}_x\text{SnS}_4$  monograin powders synthesized in  $\text{CdI}_2$  and recrystallized in KI with and without chemical etching before sulfurization.

Table 3.5. Output parameters for solar cells based on  $\text{Cu}_2\text{Zn}_{1-x}\text{Cd}_x\text{SnS}_4$  monograin powders synthesized in  $\text{CdI}_2$  and recrystallized in KI with and without chemical etching before sulfurization.

Samples	$V_{oc}$ (mV)	FF (%)	J (mA/cm <sup>2</sup> )	$\eta$ (%)
N150 non-etched	496	46.6	14.3	3.3
N150 etched	513	48.9	15.5	3.9
N150+KI non-etched	508	49.5	16.1	4.1
N150+KI etched	482	48.8	12.1	2.8

Results show that chemical etching with 1% Br in MeOH solution followed by KCN solution before post-treatment in sulfur vapor at 740 °C is beneficial for solar cell based on undoped  $\text{Cu}_2\text{Zn}_{1-x}\text{Cd}_x\text{SnS}_4$  monograin powders. All solar cell parameters were improved: open circuit voltage ( $V_{oc}$ ) increased from 496 mV to 513 mV, fill factor (FF) increased from 46.6% to 48.9%, current density ( $j_{sc}$ ) was improved from 14.3 mA/cm<sup>2</sup> to 15.5 mA/cm<sup>2</sup> and overall performance improved from 3.3% to 3.9%.

Figure 3.14 shows that  $I$ - $V$  characteristic for solar cell based on K-doped  $\text{Cu}_2\text{Zn}_{1-x}\text{Cd}_x\text{SnS}_4$  monograin powder is improved compared to solar cell based on non-etched and undoped  $\text{Cu}_2\text{Zn}_{1-x}\text{Cd}_x\text{SnS}_4$  monograin powder. The values of  $V_{oc}$  increased from 496 mV to 508 mV, FF was improved from 46.6% to 49.5% and remarkable improvement was gained in the values of  $J_{sc}$  from 14.3 to 16.1 mA/cm<sup>2</sup>. The performance of solar cell based on K-doped  $\text{Cu}_2\text{Zn}_{1-x}\text{Cd}_x\text{SnS}_4$  monograin powder improved from 3.3% to 4.1%. Results show that chemical etching for K-doped  $\text{Cu}_2\text{Zn}_{1-x}\text{Cd}_x\text{SnS}_4$  monograin powder is detrimental. It could be due to too strong etching regime, which removed the potassium containing surface layer, which was detected by XPS analysis to be on the surface of the doped crystal. The Br in methanol is very effective etchant to remove a few nanometers of surface layer on the doped monograin powder.

Results from both doping studies showed that incorporation of K in  $\text{Cu}_2\text{Zn}_{1-x}\text{Cd}_x\text{SnS}_4$  monograin powders improved the performance of solar cells. We did not observe any structural or optical changes by Raman and PL measurements, and no change in bulk composition by EDX, but XPS analysis confirmed the existent of potassium on the surface of recrystallized  $\text{Cu}_2\text{Zn}_{1-x}\text{Cd}_x\text{SnS}_4$  powder. This layer improved the solar cell efficiency up to 4.1%. Potassium doping from aqueous solution showed that optimal added K concentration is  $10^{19}$  at/cm<sup>3</sup>, which resulted in solar cell power conversion efficiency of 3.5%.

## CONCLUSIONS

The aim of this thesis was to study the influence of potassium on  $\text{Cu}_2\text{Zn}_{1-x}\text{Cd}_x\text{SnS}_4$  monograin powder structural and optical properties and monograin layer solar cell performance by using two different doping methods- an aqueous solution containing K as dopant based method and recrystallization of CZCdTS powder in KI flux. First method allowed to vary K-doping concentration from  $1 \times 10^{16}$  to  $1 \times 10^{20}$  atoms per  $\text{cm}^3$  of CZCdTS. Latter method provided more homogeneous distribution of K, but it did not allow to vary the concentration of potassium.

The doping of  $\text{Cu}_2\text{Zn}_{1-x}\text{Cd}_x\text{SnS}_4$  monograin by both solution and recrystallization method influenced the physical properties and the solar cell characteristics:

- K-doping by both methods did not show any changes in structural and optical properties by Raman and photoluminescence analysis. There were no changes in the PL band position after K-doping, but the intensity of the PL band of undoped monograin powder increased with K doping for both doping methods.
- SEM analysis showed that doping by recrystallization in KI altered the physical appearance of the crystals, with the doped crystals having a shiny appearance with smooth edges unlike the undoped crystals, which were dull with sharp edges.
- EDX analysis showed that there was no change in the bulk composition of the powder after recrystallization in KI.
- XPS analyses confirmed the existent of potassium in the surface layer of  $\text{Cu}_2\text{Zn}_{1-x}\text{Cd}_x\text{SnS}_4$  after recrystallization in KI.
- Solution doping with varying concentration of K yielded the most improved solar characteristics at concentration of  $10^{19}$  at/ $\text{cm}^3$  with efficiency from 2.8 to 3.5 %.
- The performance of solar cell based on K-doped  $\text{Cu}_2\text{Zn}_{1-x}\text{Cd}_x\text{SnS}_4$  monograin powder by recrystallization in KI flux improved from 3.3% to 4.1%.

## ABSTRACT

### Investigation of potassium doping on $\text{Cu}_2(\text{Zn,Cd})\text{SnS}_4$ monograin powder properties

The use of quaternary compounds  $\text{Cu}_2\text{ZnSnS}_4$  (CZTS),  $\text{Cu}_2\text{ZnSnSe}_4$  (CZTSe) and their solid solutions  $\text{Cu}_2\text{ZnSn}(\text{S}_x\text{Se}_{1-x})_4$  (CZTSSe) as a potential substitute for  $\text{Cu}(\text{In,Ga})(\text{S}_x\text{Se}_{1-x})_2$  have attracted increasing attention as promising absorber materials for solar cells due to their suitable physical and electronic properties, naturally abundant, inexpensive and non-toxic constituent elements. They also have tunable direct band gap between 1.0 and 1.5 eV (from pure sulfide to pure selenide compounds), and exhibits *p-type* conductivity as well as high optical absorption coefficient ( $>10^4\text{cm}^{-1}$ ). CZTS monograin powders are usually synthesized in water soluble potassium iodide flux. It means that all powders could contain some amount of K in CZTS structure as dopant. One possibility to study the influence of K on the properties of CZTS monograin powders is to substitute the K-containing flux by  $\text{CdI}_2$ . It is known that Cd from  $\text{CdI}_2$  flux incorporates to the crystals of  $\text{Cu}_2\text{ZnSnS}_4$  forming a solid solution of  $\text{Cu}_2\text{Zn}_{1-x}\text{Cd}_x\text{SnS}_4$ .

Therefore, the objective of this thesis was to investigate the influence of K-doping on the structural and optical properties of  $\text{Cu}_2\text{Zn}_{1-x}\text{Cd}_x\text{SnS}_4$ . The powder crystals were potassium doped using K-containing aqueous solution and recrystallization in KI method. XPS analysis showed that Zn substitution by Cd in the surface of the powder after recrystallization increased from 14 % to 16-17%.

K-doping of  $\text{Cu}_2\text{Zn}_{1-x}\text{Cd}_x\text{SnS}_4$  from solution and also by recrystallization in KI flux increased the intensity of the PL spectra, but no shift of the PL band position was observed by K-doping. The optimum K-doping concentration from solution for the best solar parameters was observed at  $10^{19}\text{at/cm}^3$  with power conversion efficiency of 3.5 %. Doping with increased concentration of K in the solution to  $10^{20}\text{at/cm}^3$  was detrimental to the solar cell parameters as power conversion efficiency dropped to 2.54%.

Solar cells based on  $\text{Cu}_2\text{Zn}_{1-x}\text{Cd}_x\text{SnS}_4$  monograin powders recrystallized in KI showed improvement on all output parameters. The values of  $V_{oc}$  increased from 496 mV to 508 mV,  $FF$  was improved from 46.6% to 49.5% and remarkable improvement was gained in the values of  $J_{sc}$  from 14.3 to 16.1  $\text{mA/cm}^2$ . The performance of solar cell based on K-doped  $\text{Cu}_2\text{Zn}_{1-x}\text{Cd}_x\text{SnS}_4$  monograin powder improved from 3.3% to 4.1%.

# RESÜMEE

## Kaaliumi mõju uurimine $\text{Cu}_2(\text{Zn,Cd})\text{SnS}_4$ monoterapulbri omadustele

$\text{Cu}_2\text{ZnSnS}_4$  (CZTS),  $\text{Cu}_2\text{ZnSnSe}_4$  (CZTSe) nelikühendid ja nende tahked lahused  $\text{Cu}_2\text{ZnSn}(\text{S}_x\text{Se}_{1-x})_4$  (CZTSSe) on viimasel kümnendil leidnud suurt tähelepanu absorbermaterjalidena päikeseplatereides. Tänu laialdaselt levinud ja suhteliselt odavatele koostisosadele ning mitmetele sobivatele füüsikalistele ja elektroonsetele omadustele on need materjalid üheks alternatiiviks  $\text{Cu}(\text{In,Ga})(\text{S}_x\text{Se}_{1-x})_2$  absorbermaterjalile. Sõltuvalt S ja Se suhtest on nendes ühendites võimalik varieerida keelutsooni 1,0 kuni 1,5 eV (puhtast nelikseleniidist kuni neliksulfiidini), samuti on need ühendid *p*-tüüpi juhtivusega ja omavad absorptsioonikoefitsienti  $10^4 \text{ cm}^{-1}$ .

Käesolevas töös kasutatud absorbermaterjalid olid sünteesitud monoterapulber-tehnoloogiaga. Üldjuhul sünteesitakse CZTS monoterapulber kõrgetel temperatuuridel kaaliumjodiidi (KI) sula soola (sulandaja) keskkonnas. Sellest tulenevalt sisaldavad CZTS monoterapulbri kristallid lisandina teatud määral kaaliumit, mis mõjutab saadud materjali omadusi. Üks võimalus kaaliumi mõju uurimiseks CZTS monoterapulbrite omadustele on asendada K-sisaldav sulandaja  $\text{CdI}_2$ -ga. Eelnevate uuringute tulemusel on teada, et kaadmium lisandub  $\text{CdI}_2$  sulandajast  $\text{Cu}_2\text{ZnSnS}_4$  struktuuri, moodustades  $\text{Cu}_2\text{Zn}_{1-x}\text{Cd}_x\text{SnS}_4$  tahke lahuse.

Magistritöö peamine eesmärk oli uurida kaaliumi mõju monoterapulbrilise  $\text{Cu}_2\text{Zn}_{1-x}\text{Cd}_x\text{SnS}_4$  elektrilistele ja optilistele omadustele. Kristallide legerimiseks kaaliumiga kasutati kahte erinevat meetodit: kaaliumit sisaldava vesilahusega legerimist, milles K kontsentratsiooni varieeriti  $1 \times 10^{16}$  -  $1 \times 10^{20} \text{ at/cm}^3$  ja eelnevalt  $\text{CdI}_2$  sulandajas sünteesitud  $\text{Cu}_2\text{Zn}_{1-x}\text{Cd}_x\text{SnS}_4$  rekristallisatsiooni KI sula soola keskkonnas.

XPS analüüs näitas, et pärast rekristallisatsiooni KI sulandajas suurenes Cd kontsentratsioon kristallide pinnal 14 at. %-lt 16-17 at. %-ni. K-legerimine nii vesilahusest kui ka läbi rekristallisatsiooni tõstis fotoluminestsents (PL) spektri intensiivsust, kuid PL piigi maksimumi nihkumist tänu legerimisele ei täheldatud. Leiti, et optimaalne K-legerimise lahuse kontsentratsioon on  $1 \times 10^{19} \text{ at/cm}^3$ , mille tulemusel saadi päikeselemendi kasutegur  $\eta = 3,5\%$ .

Kaaliumi kontsentratsiooni suurendamine  $1 \times 10^{20}$  at/cm<sup>3</sup> vähendas päikeseelemendi kasutegurit 2,54 %-ni.

KI sulandajas rekristallitud  $\text{Cu}_2\text{Zn}_{1-x}\text{Cd}_x\text{SnS}_4$  monoterapulbrite baasil valmistatud päikeseelemendid näitasid kõikide väljundparameetrite paranemist. Avatud vooluahela pinge ( $V_{oc}$ ) väärtus tõusis 496 mV-lt 508 mV-ni, täiteaste ( $FF$ ) paranes 46,6 %-lt 49,5 %-ni. Märkimisväärne paranemine toimus voolutihenduse väärtustes 14,3-lt kuni 16,1 mA/cm<sup>3</sup>-ni. Kaaliumiga legerimine parandas  $\text{Cu}_2\text{Zn}_{1-x}\text{Cd}_x\text{SnS}_4$  monoterapulbrite baasil valmistatud päikeseelemendi kasutegurit 3,3 %-lt 4,1 %-ni, seega omab kaalium lisandina positiivset mõju absorbermaterjali elektrilistele omadustele.

## REFERENCES

- [1] T. M. Razykov, C. S. Ferekides, D. Morel, E. Stefanakos, H. S. Ullal, and H. M. Upadhyaya, "Solar photovoltaic electricity: Current status and future prospects," *Sol. Energy*, vol. 85, no. 8, pp. 1580–1608, 2011.
- [2] A. Kitous, K. Keramidis, T. Vandyck, and B. Saveyn, "GECO 2016 Global Energy and Climate Outlook Road from Paris," 2016.
- [3] International Energy Agency IEA, "Solar Energy Perspectives," 2011.
- [4] K. Muska, "Study of Composition and Thermal Treatments of Quaternary Compounds for Monograin Layer Solar Cells," Tallinn University of Technology, 2012.
- [5] K. Jäger, O. Isabella, A.H.M. Smets, R. van Swaaij, M. Zeman, *Solar energy*, Delft University of Technology, 2014.
- [6] X. Liu, Y. Feng, H. Cui, F. Liu, X. Hao, G. Conibeer, D.B. Mitzi, M. Green, "The current status and future prospects of kesterite solar cells: A brief review," *Prog. Photovoltaics Res. Appl.*, vol. 24, no. 6, pp. 879–898, 2016.
- [7] <http://www.solar-facts-and-advice.com/solar-cells.html>.
- [8] L. El Char, L.A. Iamont, N. El Zein, "Review of photovoltaic technologies," *Renew. Sustain. Energy Rev.*, vol. 15, no. 5, pp. 2165–2175, 2011.
- [9] M. Altosaar, A. Jagomagi, M. Kauk, M. Krunks, J. Krustok, E. Mellikov, J. Raudoja, T. Varema, "Monograin layer solar cells," *Thin Solid Films*, vol. 431–432, pp. 466–469, 2003.
- [10] E. Mellikov, M. Altosaar, M. Kauk-Kuusik, K. Timmo, D. Meissner, M. Grossberg, J. Krustok, O. Volobujeva, "Growth of CZTS-Based Monograins and Their Application to Membrane Solar Cells" . K. Ito (Ed.) *Copper Zinc Tin Sulfide-Based Thin Film Solar Cells*, Wiley-VCH, pp. 289-309, 2015.
- [11] J. Fu, Q. Tian, Z. Zhou, D. Kou, Y. Meng, W. Zhou, S. Wu, "Improving the Performance of Solution-Processed  $\text{Cu}_2\text{ZnSn}(\text{S},\text{Se})_4$  Photovoltaic Materials by  $\text{Cd}^{2+}$  Substitution," *Chem. Mater.*, vol. 28, no. 16, pp. 5821–5828, 2016.
- [12] S. Chen, X. G. Gong, A. Walsh, and S. H. Wei, "Crystal and electronic band structure of  $\text{Cu}_2\text{ZnSnX}_4$  (X=S and Se) photovoltaic absorbers: First-principles insights," *Appl. Phys. Lett.*, vol. 94, no. 4, pp. 25–27, 2009.
- [13] M. Bär, B.A. Schubert, B. Marsen, R.G. Wilks, M. Blum, S. Krause, S. Poolpanratana, Y. Zhang, T. Unold, W. Yang, L. Weinhardt, C. Heske, H.W. Schock, " $\text{Cu}_2\text{ZnSnS}_4$  thin-film solar cell absorbers illuminated by soft x-rays," *J. Mater. Res.*, vol. 27, no. 8, pp. 1097–1104, 2012.
- [14] Z. Tong, C. Yan, Z. Su, F. Zeng, J. Yang, Y. Li, L. Jiang, Y. Lai, F. Liu, "Effects of potassium doping on solution processed kesterite  $\text{Cu}_2\text{ZnSnS}_4$  thin film solar cells," *Appl. Phys. Lett.*, vol. 105, no. 22, 2014.
- [15] I. Klavina, T. Kaljuvee, K. Timmo, J. Raudoja, R. Traksmäa, M. Altosaar, D. Meissner, "Study of  $\text{Cu}_2\text{ZnSnSe}_4$  monograin formation in molten KI starting from binary chalcogenides," *Thin Solid Films*, vol. 519, no. 21, pp. 7399–7402, 2011.
- [16] K. Timmo, M. Altosaar, M. Kauk, J. Raudoja, E. Mellikov, "CuInSe<sub>2</sub> monograin growth in the liquid phase of potassium iodide," *Thin Solid Films*, vol. 515, no. 15, pp. 5884–5886, 2007.
- [17] K. Timmo, M. Altosaar, J. Raudoja, E. Mellikov, T. Varema, M. Danilson, M. Grossberg, "The effect of sodium doping to CuInSe<sub>2</sub> monograin powder properties," vol. 515, pp.

- 5887–5890, 2007.
- [18] [http://www.elements.nb.ca/theme/renewable\\_energy/jacob/moeller.htm](http://www.elements.nb.ca/theme/renewable_energy/jacob/moeller.htm)
- [19] <http://bestsale2u.com/photovoltaic-cell-working-principle-how-to-convert-sunlight-into-electricity/>
- [20] EPIA, “Solar Generation 6 Solar Photovoltaic Electricity,” 2011.
- [21] K. Ito, *Copper Zinc Tin Sulfide-Based Thin-Film Solar Cells*. Nagano: John Wiley & Sons, Ltd, 2015.
- [22] M. A. Green, “Photovoltaic principles,” *Phys. E*, vol. 14, no. 1–2, pp. 11–17, 2002.
- [23] D. A. Sproul, “Understanding the *p-n* Junction,” *Corp. Commun. An Int. J.*, vol. 3, no. 4, pp. 341–355, 2007.
- [24] B. Ananthoju, J. Mohapatra, M.K. Jangid, D. Bahadur, N.V. Medhekar, and M. Aslam, “Cation/Anion Substitution in  $\text{Cu}_2\text{ZnSnS}_4$  for Improved Photovoltaic Performance,” *Sci. Rep.*, vol. 6, no. September, p. 35369, 2016.
- [25] A. Fischereder, T. Rath, W. Haas, H. Amenitsch, J. Albering, D. Meischler, S. Larissegger, M. Edler, R. Saf, F. Hofer, G. Trimmel, “Investigation of  $\text{Cu}_2\text{ZnSnS}_4$  formation from metal salts and thioacetamide,” *Chem. Mater.*, vol. 22, no. 11, pp. 3399–3406, 2010.
- [26] Fraunhofer Institute for Solar and Systems, “Photovoltaics report,” 2016.
- [27] E. Ghorbani, J. Kiss, H. Mirhosseini, M. Schmidt, J. Windeln, T.D. Kühne, C. Felser, “Insights into Intrinsic Defects and the Incorporation of Na and K in the  $\text{Cu}_2\text{ZnSnSe}_4$  Thin-Film Solar Cell Material from Hybrid-Functional Calculations,” *J. Phys. Chem. C*, vol. 120, no. 4, pp. 2064–2069, 2016.
- [28] G. Nkwusi, M. Altosaar, E. Mellilov, I. Leinemann, J. Raudoja, V. Mikli, M. Kauk-Kuusik, “Synthesis of  $\text{Cu}_2(\text{ZnCd})\text{SnS}_4$  Absorber Material for Monograin Membrane Applications,” *Cambridge Univ Press*, vol. 2, pp. 1–6, 2014.
- [29] N. Muhunthan, O.P. Singh, M.K. Thakur, P. Karthikeyan, D. Singh, m. Saravanan, V.N. Singh, “Interfacial Properties of CZTS Thin Film Solar Cell,” *J. Sol. Energy*, vol. 2014, pp. 1–8, 2014.
- [30] Y. T. Hsieh, G. Han, C. Jiang, T-B. Song, H. Chen, L. Meng, H. Zhou, Y. Yang, “Efficiency Enhancement of  $\text{Cu}_2\text{ZnSn}(\text{S},\text{Se})_4$  Solar Cells via Alkali Metals Doping,” *Adv. Energy Mater.*, vol. 6, no. 7, pp. 1–6, 2016.
- [31] K. L. Chopra, P. D. Paulson, V. Dutta, “Thin-film solar cells: an overview,” *Prog. photovoltaics*, vol. 12, no. 23, pp. 69–92, 2004.
- [32] S. Li, “Optimization of Buffer Layer for Copper-Zinc-Tin-Sulfide-based Solar Cells,” Tallinn University of Technology, 2016.
- [33] K. Timmo, M. Altosaar, J. Raudoja, K. Muska, M. Pilvet, M. Kauk, T. Varema, M. Danilson, O. Volobujeva, E. Mellikov, “Sulfur-containing  $\text{Cu}_2\text{ZnSnSe}_4$  monograin powders for solar cells,” *Sol. Energy Mater. Sol. Cells*, vol. 94, no. 11, pp. 1889–1892, 2010.
- [34] C.-J. Wang, S.-C. Shei, S.-J. Chang, “Synthesis and characterization of CZTSe nanoinks using polyetheramine as solvent,” *Opt. Mater. Express*, vol. 4, no. 8, p. 1593, 2014.
- [35] E. Mellikov, E. Mellikov, D. Meissner, M. Altosaar, M. Kauk, J. Krustok, A. Öpik, O. Volobujeva, J. Iljina, K. Timmo, I. Klavina, J. Raudoja, M. Grossberg, T. Varema, K. Muska, M. Ganchev, S. Bereznev, M. Danilson, “CZTS Monograin Powders and Thin Films,” *Adv. Mater. Research.*, vol. 222, pp. 8–13, 2011.
- [36] A.S. Oyewo, “Chemical Modification of  $\text{Cu}_2\text{ZnSn}(\text{S},\text{Se})_4$  Solar Cell Absorber Surface

- Before *p-n* junction Formation,” Tallinn University of Technology, 2015.
- [37] E. Kask, “Study of Kesterite Solar Cell Absorbers by Capacitance Spectroscopy Methods,” Tallinn University of Technology, 2016.
- [38] E. Mellikov, D. Meissner, T. Varema, M. Altosaar, M. Kauk, O. Volobujeva, J. Raudoja, K. Timmo, M. Danilson., “Monograin materials for solar cells,” *Sol. Energy Mater. Sol. Cells*, vol. 93, no. 1, pp. 65–68, 2009.
- [39] G. Nkwusi, I. Leinemann, M. Grossberg, M. Altosaar, D. Meissner, “Formation Of Copper Zinc Tin Sulfide In Cadmium Iodide For Monograin Membrane Solar cells,” *Cysni Conf. Lith.*, vol. 2, pp. 1–10, 2012.
- [40] I. Leinemann, J. Raudoja, M. Grossberg, R. Traksmaa, T. Kaljuvee, M. Altosaar, D. Meissner, “Comparison of copper zinc tin selenide formation in molten potassium iodide and sodium iodide as flux materials.,” in *In: Proceedings of the Conference of Young Scientists on Energy Issues, Kaunas, Lithuania*, 2010, pp. 1–8.
- [41] R. B. V. Chalapathy, G. S. Jung, Y. M. Ko, B. T. Ahn, and H. Kwon, “Fabrication of  $\text{Cu}_2\text{ZnSnS}_4$  Films by Rapid Thermal Annealing of Cu/ZnSn/Cu Precursor Layer and Their Application to Solar Cells,” *Curr. Photovolt. Res.*, vol. 1, no. 2, pp. 82–89, 2013.
- [42] K. Muska, M. Kauk, M. Altosaar, M. Pilvet, M. Grossberg, and O. Volobujeva, “Synthesis of  $\text{Cu}_2\text{ZnSnS}_4$  monograin powders with different compositions,” *Energy Procedia*, vol. 10, pp. 203–207, 2011.
- [43] W. Li, J. Chen, C. Yan, and X. Hao, “The effect of ZnS segregation on Zn-rich CZTS thin film solar cells,” *J. Alloys Compd.*, vol. 632, pp. 178–184, 2015.
- [44] A. Walsh, S. Chen, X.G. Gong, S-H. Wei, “Crystal structure and defect reactions in the kesterite solar cell absorber  $\text{Cu}_2\text{ZnSnS}_4$  (CZTS): Theoretical insights,” *AIP Conf. Proc.* vol. 1399, pp. 63–64, 2011.
- [45] S. Chen, X. G. Gong, A. Walsh, S. H. Wei, “Defect physics of the kesterite thin-film solar cell absorber  $\text{Cu}_2\text{ZnSnS}_4$ ,” *Appl. Phys. Lett.*, vol. 96, no. 2, pp. 8–10, 2010.
- [46] M. Dimitrievska, A. Fairbrother, E. Saucedo, A. Pérez-Rodríguez, V. Izquierdo-Roca, “Influence of compositionally induced defects on the vibrational properties of device grade  $\text{Cu}_2\text{ZnSnSe}_4$  absorbers for kesterite based solar cells,” *Appl. Phys. Lett.*, vol. 106, no.7, 2015.
- [47] A. Emrani, P. Vasekar, C. R. Westgate, “Effects of sulfurization temperature on CZTS thin film solar cell performances,” *Sol. Energy*, vol. 98, no. PC, pp. 335–340, 2013.
- [48] M. Kauk, K. Muska, M. Altosaar, J. Raudoja, M. Pilvet, T. varema, K. Timmo, O. Volobujeva, “Effects of sulphur and tin disulphide vapour treatments of  $\text{Cu}_2\text{ZnSnS}(\text{Se})_4$  absorber materials for monograin solar cells,” *Energy Procedia*, vol. 10, pp. 197–202, 2011.
- [49] X. Liu, J. Huang, F. Zhou, F. Liu, K. Sun, C. Yan, J.A. Stride, X. Hao, “Understanding the Key Factors of Enhancing Phase and Compositional Controllability for 6% Efficient Pure-Sulfide  $\text{Cu}_2\text{ZnSnS}_4$  Solar Cells Prepared from Quaternary Wurtzite Nanocrystals,” *Chem. Mater.*, vol. 28, no. 11, pp. 3649–3658, 2016.
- [50] I. Repins, N. Vora, C. Beall, S-H. Wei, Y. Yan, M. Romero, G. Teeter, H. Du, B. To, M. Young, R. Noufi, “Kesterites and Chalcopyrites: A Comparison of Close Cousins,” *MRS Proc.*, vol. 1324, no. group II, p. mrss11-1324-d17-01, 2011.
- [51] A. Walsh, S. Chen, X.G. Gong, S.H. Wei, “Crystal structure and defect reactions in the kesterite solar cell absorber  $\text{Cu}_2\text{ZnSnS}_4$  (CZTS): Theoretical insights,” *AIP Conf. Proc.*, vol. 1399, no. 2011, pp. 63–64, 2011.

- [52] M. Grossberg, J. Krustok, J. Raudoja, T. Raadik, "The role of structural properties on deep defect states in  $\text{Cu}_2\text{ZnSnS}_4$  studied by photoluminescence spectroscopy," *Appl. Phys. Lett.*, vol. 101, no. 2012, p. 102102, 2012.
- [53] J.J.S. Scragg, L. Choubrac, A. Lafond, T. Ericson, C. Platzer-Björkman, "A low-temperature order-disorder transition in  $\text{Cu}_2\text{ZnSnS}_4$  thin films," *Appl. Phys. Lett.*, vol. 104, no. 4, pp. 1–5, 2014.
- [54] A. Nagoya, R. Asahi, R. Wahl, G. Kresse, "Defect formation and phase stability of  $\text{Cu}_2\text{ZnSnS}_4$  photovoltaic material," *Phys. Rev. B - Condens. Matter Mater. Phys.*, vol. 81, no. 11, pp. 1–4, 2010.
- [55] S. Chen, L.W. Wang, A. Walsh, X.G. Gong, S.H. Wei, "Abundance of  $\text{CuZn}+\text{SnZn}$  and  $2\text{CuZn}+\text{SnZn}$  defect clusters in kesterite solar cells," *Appl. Phys. Lett.*, vol. 101, no. 22, p. 223901, 2012.
- [56] S. Chen, J.H. Yang, X. G. Gong, A. Walsh, S. H. Wei, "Intrinsic point defects and complexes in the quaternary kesterite semiconductor  $\text{Cu}_2\text{ZnSnS}_4$ ," *Phys. Rev. B - Condens. Matter Mater. Phys.*, vol. 81, no. 24, pp. 35–37, 2010.
- [57] S. Chen, A. Walsh, X.G. Gong, S.H. Wei, "Classification of lattice defects in the kesterite  $\text{Cu}_2\text{ZnSnS}_4$  and  $\text{Cu}_2\text{ZnSnSe}_4$  earth-abundant solar cell absorbers," *Adv. Mater.*, vol. 25, no. 11, pp. 1522–1539, 2013.
- [58] G. Nkwusi, I. Leinemann, M. Altosaar, "The Processes and Enthalpies in Synthesis of  $\text{Cu}_2\text{ZnSnS}_4$  in Molten  $\text{CdI}_2$ ," *Int. Adv. Res. J. Sci. Eng. Technol.*, vol. 3, no. 5, 2016.
- [59] S. Fu, Q. Tian, Z. Zhou, D. Kou, Y. Meng, W. Zhou, S. Wu, "Improving the Performance of Solution-Processed  $\text{Cu}_2\text{ZnSn}(\text{S},\text{Se})_4$  Photovoltaic Materials by  $\text{Cd}^{2+}$  Substitution," *Chem. Mater.*, vol. 28, no. 16, p. 5821–5828., 2016.
- [60] Q. Zhang, H. Deng, L. Chen, L. Yu, J. Tao, L. Sun, P. Yang, J. Chu, "Cation substitution induced structural transition, band gap engineering and grain growth of  $\text{Cu}_2\text{Cd}_x\text{Zn}_{1-x}\text{SnS}_4$  thin films," *Journal of Alloys and Compounds*, vol. 695, no. 25, pp. 482-488, 2017
- [61] C. Yan, K. Sun, J. Huang, S. Johnston, F. Liu, B.P. Veetil, K. Sun, A. Pu, F. Zhou, J.A. Stride, M.A. Green, X. Hao, "Beyond 11% Efficient Sulfide Kesterite  $\text{Cu}_2\text{Zn}_x\text{Cd}_{1-x}\text{SnS}_4$  Solar Cell: Effects of Cadmium Alloying," *ACS Energy Lett.*, no. May, pp. 930–936, 2017.
- [62] M. Pilvet, M. Kauk-Kuusik, M. Altosaar, M. Grossberg, M. Danilson, K. Timmo, A. Mere, V. Mikli, "Compositionally tunable structure and optical properties of  $\text{Cu}_{1.85}(\text{Cd}_x\text{Zn}_{1-x})_{1.1}\text{SnS}_{4.1}$  ( $0 \leq x \leq 1$ ) monograin powders," *Thin Solid Films*, vol. 85, pp. 1–4, 2014.
- [63] U. Pol, R.P. Rumelt, O. Costa, *Semiconductor Technology*, 2003.
- [64] [https://en.wikibooks.org/wiki/Semiconductor\\_Electronics/Semiconductor/Doping](https://en.wikibooks.org/wiki/Semiconductor_Electronics/Semiconductor/Doping), "Semiconductor Electronics," 2017.
- [65] T. Maeda, A. Kawabata, T. Wada, "First-principles study on alkali-metal effect of Li, Na, and K in  $\text{Cu}_2\text{ZnSnS}_4$  and  $\text{Cu}_2\text{ZnSnSe}_4$ ," *Phys. Status Solidi*, vol. 12, no. 6, pp. 631–637, 2015.
- [66] C.M. Sutter-Fella, J.A. Stückelberger, H. Hagendorfer, F.L. Mattina, L. Kranz, S. Nishiwaki, A.R. Uhl, Y.E. Romanyuk, A.N. Tiwari, "Sodium Assisted Sintering of Chalcogenides and Its Application to Solution Processed  $\text{Cu}_2\text{ZnSn}(\text{S},\text{Se})_4$  Thin Film Solar Cells," *Chem. Mater.*, vol. 26, no. 3, pp. 1420–1425, 2014.
- [67] S. López-Marino, Y. Sánchez, M. Espíndola-Rodríguez, X. Alcobé, H. Xie, M. Neuschitzer, I. Becerril, S. Giraldo, M. Dimitrievska, M. Placidi, L. Fourdrinier,

- V.Izquierdo-Roca, A. Pérez-Rodríguez, E. Saucedo, “Alkali doping strategies for flexible and light-weight  $\text{Cu}_2\text{ZnSnSe}_4$  solar cells,” *J. Mater. Chem. A*, vol. 4, pp. 1895–1907, 2016.
- [68] M. Kauk-Kuusik, K. Timmo, M. Danilson, M. Altosaar, M. Grossberg, K. Ernits, “*p-n* junction improvements of  $\text{Cu}_2\text{ZnSnS}_4/\text{CdS}$  monograin layer solar cells,” *Appl Surf Sci.*, no. 357, p. 795–798., 2015.
- [69] B. B. A. Rockett, J.S. Britt, T. Gillespie, C. Marshall, M.M. Al Jassim, F. Hasoon, R. Matson, “Na in selenized  $\text{Cu}(\text{In,Ga})\text{Se}_2$  on Na-containing and Na-free glasses: distribution, grain structure, and device performances,” *Thin Solid Films*, vol. 372, no. 1–2, pp. 212–217, 2000.
- [70] N. Xu, P. Li, Y. Hao, X. Wang, and L. Meng, “Effect of sputtering power on Cd / Zn atomic ratio and optical properties of  $\text{Cu}_2\text{Zn}_x\text{Cd}_{1-x}\text{SnS}_4$  thin films deposited by magnetron sputtering : An experimental and first-principle study,” vol. 660, pp. 132–135, 2016.
- [71] M. Grossberg, J. Krustok, J. Raudoja, K. Timmo, M. Altosaar, and T. Raadik, “Photoluminescence and Raman study of  $\text{Cu}_2\text{ZnSn}(\text{Se}_x\text{S}_{1-x})_4$  monograins for photovoltaic applications,” *Thin Solid Films*, vol. 519, no. 21, pp. 7403–7406, 2011.
- [72] K. Timmo, M. Kauk-Kuusik, M. Pilvet, T. Raadik, M. Altosaar, M. Danilona, M. Grossberg, J. Raudoja, K. Ernits, “Influence of order-disorder in  $\text{Cu}_2\text{ZnSnS}_4$  powders on the performance of monograin layer solar cells,” *Thin Solid Films*, 2016.
- [73] P. Jackson, R. Wuerz, D. Hariskos, E. Lotter, W. Witte, M. Powalla, “Effects of heavy alkali elements in  $\text{Cu}(\text{In,Ga})\text{Se}_2$  solar cells with efficiencies up to 22.6%,” *Phys. Status Solidi - Rapid Res. Lett.*, vol. 10, no. 8, pp. 583–586, 2016.

## **ACKNOWLEDGEMENT**

Thanks to God for the gift of life and wisdom for the success of this thesis.

I wish to express my deep gratitude to my supervisor Dr. Marit Kauk-Kuusik (Senior Research Scientist), for her understanding, patience and tireless effort throughout my research work.

I thank my co-supervisor Dr. Kristi Timmo (Senior Research Scientist) and Godswill Nkwusi for their dedication and guidance all through this project. They really helped me to understand the concept of this thesis. My special appreciation also goes Dr. Mare Altosaar (Senior Research Scientist) who kept her doors open to me for assistance at every point in time.

I am grateful to all members of this research group who have contributed to my thesis: Maris Pilvet, Dr. Valdek Mikli, Dr. Mati Danilson, Dr. Maarja Grossberg, Dr. Jaan Raudoja, Dr. Tiit Varema and Suresh Kumar.

I also appreciate Dr. Nicolai Spalatu who agreed to review this master thesis.

Lastly, I thank my family members for understanding my busy schedule during this project and my colleagues (Kang and Denisa) for their support.